# Wildfire smoke offsets decades of progress in reducing ozone exposure across the United States

Minghao Qiu[1,2#*], Yangmingkai Li[1#], Marissa Childs[3], Makoto Kelp[4], Xiaomeng Jin[5], Guanyu Huang[1,2,6], Mahdieh Danesh Yazdi[2,6], Yaguang Wei[7], Yuan Wang[8], Kai Chen[9,10]

**1** School of Marine and Atmospheric Sciences, Stony Brook University, Stony Brook, NY, U.S.A.

**2** Program in Public Health, Stony Brook University, Stony Brook, NY, U.S.A.

**3** Department of Environmental & Occupational Health Sciences, University of Washington, Seattle, WA, U.S.A.

**4** Department of Atmospheric Sciences, University of Utah, Salt Lake City, UT, U.S.A.

**5** Department of Environmental Sciences, Rutgers, The State University of New Jersey, New Brunswick, NJ, U.S.A.

**6** Department of Family, Population, and Preventive Medicine, Stony Brook University, Stony Brook, NY, U.S.A.

**7** Department of Environmental Medicine, Icahn School of Medicine at Mount Sinai, New York, NY, U.S.A.

**8** Department of Earth System Science, Stanford Doerr School of Sustainability, Stanford University, Stanford, CA, U.S.A.

**9** Department of Environmental Health Sciences, Yale School of Public Health, New Haven, CT, U.S.A.

**10** Yale Center on Climate Change and Health, Yale School of Public Health, New Haven, CT, U.S.A.

[#] These authors contributed equally.

[*] To whom correspondence should be addressed. E-mail: minghao.qiu@stonybrook.edu

# Abstract

Ground-level ozone ($O_3$) pollution has declined in the U.S., yet the progress has stalled in recent years, coinciding with increasing wildfire smoke. Using ensemble machine learning models trained on surface observations, we develop a gridded daily smoke $O_3$ dataset across the contiguous U.S. from 2006-2023. We estimate that wildfire smoke placed an additional 29 million people each year in areas exceeding the federal $O_3$ standard, a 74% increase over a no-smoke baseline. Smoke has offset 36% of the reduction in the $O_3$ nonattainment population and 62% of the improvement in population-weighted $O_3$ concentrations over 2006-2023. Smoke $O_3$ follows spatial-temporal patterns distinct from smoke $PM_{2.5}$. Wildfire smoke is increasingly eroding the $O_3$ health benefits achieved through decades of emission controls, posing a growing challenge for air quality management in a changing climate.

# Introduction

Ozone ($O_3$) is one of six criteria air pollutants regulated under the Clean Air Act in the U.S., and is the leading pollutant responsible for nonattainment of the National Ambient Air Quality Standards (NAAQS) by both population and number of counties affected (*1*). Exposure to $O_3$ increases the risk of respiratory conditions such as asthma and chronic obstructive pulmonary disease (*2*), cardiovascular disease (*3*, *4*), and premature mortality (*5*, *6*). Ground-level $O_3$ concentrations have continuously declined since the 1990s, especially in the eastern U.S. during summer (*7–12*). However, this progress has stagnated in recent years at the national level (*13*, *14*). Prior research has suggested this is due to a combination of increasing heat extremes (*13*), slowdown in reducing anthropogenic nitrogen oxides ($NO_x$) and volatile organic compound (VOC) emissions (*15*, *16*), and background $O_3$ changes (*10*, *17*). This stalled progress also coincides with increasing wildfire smoke, which has grown substantially over the past three decades (*18–21*). Existing research has extensively focused on smoke fine particulate matter ($PM_{2.5}$) and has found that wildfire smoke has reversed the otherwise declining trend in $PM_{2.5}$ (*19*, *20*, *22–24*). However, the effects of wildfire smoke on U.S. $O_3$ trends and population exposure have not been quantified, due to the complex pathways through which wildfires affect $O_3$ and the lack of spatially complete estimates of smoke $O_3$ concentrations.

Wildfires can impact ground-level $O_3$ through emissions of precursor species, long-range transport, and radiative and chemical effects from smoke aerosols, with the net effect varying across space and time depending on the local chemical environment and meteorological conditions (*25–29*). Recent studies suggest that the wildfire impacts on $O_3$ are substantial and growing in the U.S. Lee and Jaffe found that surface $O_3$ increases by an average of 8 ppb on smoke days (days when satellite imagery identifies overhead smoke plumes) across U.S. monitors during 2018-2023 (*30*), and Li et al. estimated that smoke $O_3$ led to over 2,000 excess deaths annually using interpolated data from monitor measurements (*31*). Existing research has quantified smoke contributions to ground-level $O_3$ over monitoring locations across the U.S. (*30–33*), or has developed gridded smoke $O_3$ data at local or regional scales (*34*, *35*). However, a spatially complete, long-term smoke $O_3$ dataset across the U.S. does not exist to support analysis of trends, distributions, population exposure, and health burden associated with smoke $O_3$ nationally.

Quantifying wildfire influences on population exposure to $O_3$ requires overcoming several methodological challenges that have been identified in the existing literature. Two general approaches have

been used to estimate wildfire smoke contributions to air pollution and population exposure. The first relies on process-based chemical transport models (CTMs) driven by fire emissions inventories to simulate smoke pollutant concentrations (*36*, *37*). The second uses statistical or machine learning (ML) methods that relate surface observations to smoke indicators, remotely sensed atmospheric composition, fire, and meteorological predictors (*20*, *23*, *38*, *39*). Both approaches face important limitations for smoke $O_3$ estimations. CTMs are subject to high uncertainty in wildfire emissions inventories (*37*, *40*), and often rely on chemical mechanisms that may not adequately capture $O_3$ formation in smoke plumes (*41*). ML approaches can more closely reproduce observed surface pollution during smoke events, but may perform less well in areas with sparse monitoring coverage and may miss the impacts of diffuse smoke altogether (*42*). For ML approaches, accounting for meteorological conditions on smoke days is particularly important for $O_3$, as smoke days tend to have higher temperatures and greater UV radiation that separately promote $O_3$ formation (*31*).

In this study, we develop a daily gridded dataset that quantifies wildfire smoke impacts on the surface $O_3$ at daily and 10 km resolutions across the contiguous U.S. from 2006-2023. To leverage the strengths of observation-based approaches while accounting for the meteorological confounding identified above, we train two sets of ensemble ML models (Figure 1): (1) a smoke model that predicts Maximum Daily 8-hour Average (MDA8) $O_3$ on smoke days, and (2) a non-smoke model that estimates counterfactual $O_3$ concentrations under the same meteorological conditions but in the absence of fire smoke. Smoke days are identified using satellite-derived smoke plumes generated from the National Oceanic and Atmospheric Administration (NOAA) Hazard Mapping System (HMS) following prior literature, with sensitivity analyses conducted using alternative smoke day definitions. Both models predict MDA8 $O_3$ concentrations from U.S. Environmental Protection Agency's (EPA) AirData repository using meteorological variables, surface nitrogen dioxide and formaldehyde (as proxies for $O_3$ precursors), and geographical features as predictors. The smoke model additionally incorporates fire-related variables including fire radiative power, distance to fires, and satellite-derived smoke $PM_{2.5}$ estimates. Smoke $O_3$ is defined as the difference between predicted $O_3$ and estimated counterfactual non-smoke $O_3$ on each smoke day. Using this dataset, we quantify wildfire smoke contributions to population $O_3$ exposure and NAAQS nonattainment across the U.S. We further examine the spatial and temporal relationship between smoke $O_3$ and smoke $PM_{2.5}$ to assess whether smoke $O_3$ represents a distinct health risk in addition to smoke PM2.5 exposure. Compared to prior monitor-based estimates of smoke $O_3$ (*30–33*), our gridded dataset provides spatially complete coverage over a longer time horizon.

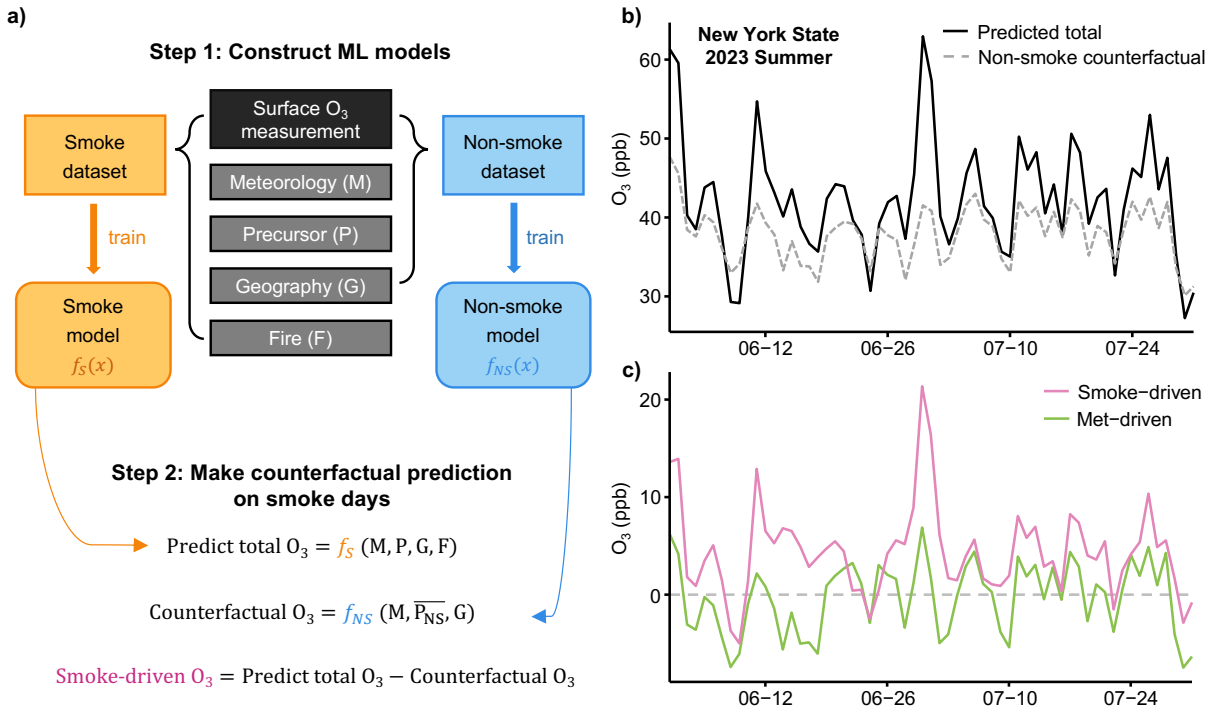


Figure 1: **Schematic figure of our machine learning-based approach for estimating smoke $O_3$ concentrations.** Panel a: In Step 1, we construct two machine learning models (smoke and non-smoke) to predict $O_3$ concentrations. The smoke model is only trained on the smoke dataset (i.e., all grid-days with smoke influences) to predict total $O_3$ concentration (both smoke and non-smoke) on smoke days. The non-smoke model is only trained on the non-smoke dataset (i.e., all grid-days with no smoke influences) to predict total $O_3$ concentration on non-smoke days, and thus used to predict counterfactual non-smoke $O_3$ on smoke days. In Step 2, we use these models to estimate the total $O_3$ concentration and counterfactual $O_3$ concentrations on smoke days. Panel b: an illustration of our method for New York State during summer 2023 (averaged over all grid cells in New York State). The plot shows predicted total $O_3$ concentration ("predicted total", black line) and estimated counterfactual non-smoke $O_3$ using smoke-day meteorology (grey dashed line). Panel c: the plot shows smoke-driven $O_3$ changes (pink line) calculated as the difference between predicted total and counterfactual $O_3$, and met-driven $O_3$ changes (green line) calculated as the impacts of meteorological variability on $O_3$ concentrations in New York State during summer 2023.

# Results

## Model Performance and Validations

Our non-smoke ensemble model achieved an $R^2$ of 0.73 and an RMSE of 7.28 ppb in predicting MDA8 $O_3$ on non-smoke days (Table 1, Table S1, Figure S1). The model performs well across most

of the contiguous U.S., with relatively lower performance at monitoring locations along the U.S. West Coast and parts of the Mountain West (Figure S2). The lower performance in the Mountain West may reflect relatively sparser monitoring coverage over complex terrain and episodic stratospheric $O_3$ intrusions at high-elevation sites (*7*, *17*, *43*). The lower performance in the U.S. West Coast may be due to variable coastal meteorological dynamics (*17*) and a complex emissions and chemical landscape (*44*). Performance remains similar under a more stringent 150 km spatial CV split (Figure S2), suggesting that our model generalizes to locations farther from training monitors. The strong out-of-sample performance of the non-smoke model, as well as the overlap in predictors between smoke and non-smoke days (Figure S3), provides confidence in its use for estimating counterfactual non-smoke $O_3$ on smoke days under observed meteorological conditions.

Table 1: Out-of-sample performance metrics of smoke and non-smoke $O_3$ models, reported based on spatial cross-validation at 75 km resolution. Within $R^2$ is calculated from linear regressions that include station and month fixed effects, thus capturing the model's ability to capture spatio-temporal variability beyond seasonality and time-invariant location differences. Warm season is defined as April to September.

| **Model** | $R^2$ | **Within** $R^2$ | **RMSE (ppb)** | **MAE (ppb)** |
|---|---|---|---|---|
| Non-smoke (all-year) | 0.73 | 0.57 | 7.28 | 5.47 |
| Non-smoke (warm-season) | 0.68 | 0.56 | 7.98 | 6.05 |
| Smoke (no interpolation) | 0.73 | 0.64 | 7.39 | 5.50 |
| Smoke (with interpolation) | 0.85 | 0.81 | 5.73 | 4.07 |

Our smoke ensemble model predicts MDA8 $O_3$ on smoke days with reasonable accuracy ($R^2$ = 0.73, within $R^2$ = 0.64, RMSE = 7.39 ppb; Table 1, Table S1, Figure S1). The smoke model achieves comparable performance to the non-smoke model across the eastern U.S. but performs worse in the western U.S. (Figures S2 and S4). The lower performance in the western U.S. may reflect $O_3$ formation in smoke plumes through complex photochemistry that depends on fire-emitted VOC speciation, fuel characteristics, plume age, and local $NO_x$ regimes (*26*, *41*). These factors are not directly captured by the fire-related predictors in our ML models, and most are available only from individual field campaigns rather than data products across the U.S. We find that including interpolated $O_3$ concentrations from nearby surface monitors (see Methods) as an additional predictor achieves substantially higher predictive accuracy in the western U.S. (Figure S5), with interpolated $O_3$ as the most important feature (Figures S6 and S7). However, the heavy reliance on a single

feature raises concerns about overfitting and spatial artifacts (Figure S8). Nevertheless, the general pattern and population-level exposure in predicted $O_3$ remain highly similar across interpolation and non-interpolation models (Figure S9). We therefore use the non-interpolation smoke model as our primary model for estimating smoke $O_3$. Importantly, we also find that the prediction bias of $O_3$ generally has the same sign in >85% of the monitor locations, resulting in lower bias when calculating smoke $O_3$ as the differences between the two sets of predictions (Figure S10).

## Wildfire smoke contribution to ground-level $O_3$

Wildfire smoke leads to widespread increases in surface $O_3$ across the contiguous U.S., with a growing contribution over time (Figure 2). These spatial patterns are broadly consistent with prior monitor-based estimates (*30–32*). During 2006-2022, smoke-driven $O_3$ enhancement was mostly observed in the western U.S., where wildfires are most active, and in the downwind Midwest, with strong interannual variability driven by active fire years such as 2017, 2018, 2020, and 2021. The Midwest consistently exhibits the highest smoke $O_3$ levels, as it is directly downwind of smoke from fires that occurred in the western U.S. and Canada. Wildfire smoke impacts on $O_3$ peaked in 2023, when the entire Midwest and Southern U.S., as well as parts of the Northeastern U.S., experienced elevated $O_3$ driven by widespread transport of Canadian wildfire smoke. Wildfire smoke increased the annual mean $O_3$ concentrations by up to 5 ppb in 2023 in the Midwest (see Figure S11 for modeled $O_3$ levels at selected stations in summer 2023). These results are consistent with prior analyses based on airborne and surface measurements over the Midwest during the 2023 Canadian smoke events (*45–47*). Airborne measurements and modeling studies have shown that ground-level $O_3$ increases during smoke episodes due to direct transport of $O_3$, transport of reactive nitrogen species, and $O_3$ production from VOCs in smoke plumes reacting with local $NO_x$ (*27*, *46*, *48*).

We found that smoke has offset what would otherwise be a declining trend in population exposure to $O_3$ pollution across the U.S. We calculated the population-weighted $O_3$ "design value" (i.e., annual 4th-highest MDA8 $O_3$ concentration) and the number of people living in nonattainment areas ($O_3$ design value exceeding 70 ppb), following the NAAQS criterion (Figure 3; Table S2). Absent smoke influence, the population-weighted $O_3$ design value would decline by 8.2 ppb at the national level (from 68.1 ppb in 2006-2008 to 59.9 ppb in 2021-2023), and the annual nonattainment population would fall from 100.6 million in 2006–2008 to 14.7 million in 2021–2023. Rising wildfire smoke has offset 36% of the reduction in nonattainment population, 40% of the reduction in design value, and 62% of the improvement in population-weighted $O_3$ concentrations over the same period.

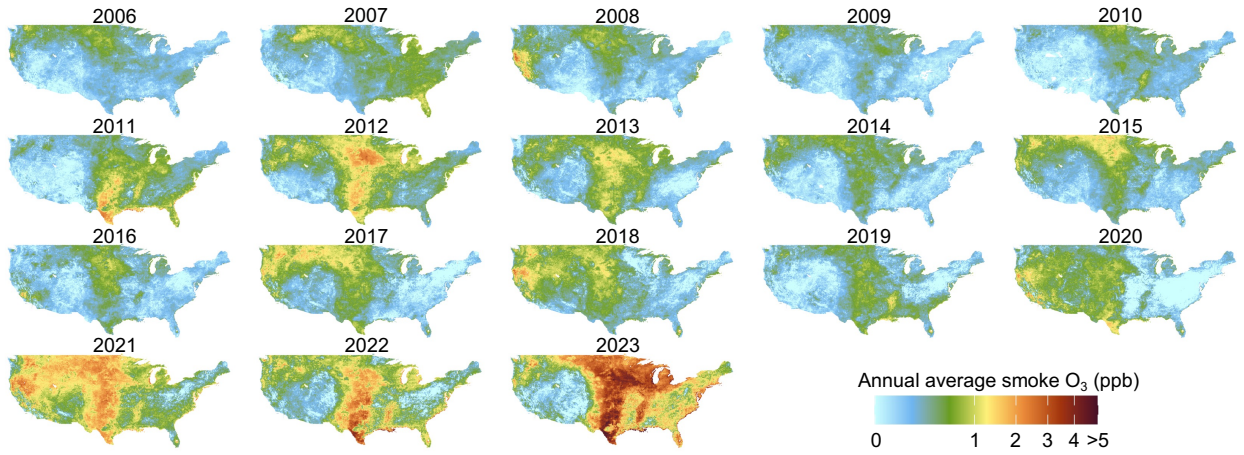


Figure 2: **Wildfire smoke contribution to annual average $O_3$ concentrations across the U.S. from 2006 to 2023.** Wildfire smoke contribution to annual average $O_3$ concentrations is calculated using "smoke-driven" $O_3$ estimates averaged over all days in a year (smoke $O_3$ is assumed to be zero on non-smoke days).

We estimate that wildfire smoke has placed an additional 29 million people in nonattainment on average each year during 2006–2023, a 74% increase over the non-smoke baseline. Smoke-driven nonattainment regions are concentrated in the western U.S., Midwest, and northeastern U.S. (Figure S12). Smoke also contributes substantially to daily $O_3$ exceedance events, defined as days when MDA8 $O_3$ exceeds the 70 ppb NAAQS threshold (Figure S13).

Our estimates of smoke-driven $O_3$ isolated the contribution of fire smoke after accounting for the meteorological differences between smoke and non-smoke days. We found that not accounting for the meteorological variability between smoke and non-smoke days (e.g., higher ambient temperature and higher UV radiation on smoke days) would over-inflate our smoke $O_3$ estimates by 39% (Figure S14). To better quantify smoke impacts on $O_3$ through different mechanisms, we further decomposed the smoke-driven $O_3$ into changes due to increases in $O_3$ precursors ($NO_2$ and HCHO) and a residual component, by constructing an additional counterfactual prediction that allows $NO_2$ and HCHO concentrations to vary with smoke-day conditions (rather than using non-smoke average values). We found that changes in $O_3$ precursors account for 63% of the total smoke-driven $O_3$, with the remainder likely associated with direct transport of $O_3$ (*46*). Contributions from precursor changes almost dominate the smoke $O_3$ burden in regions closer to active fires (Figure S14).

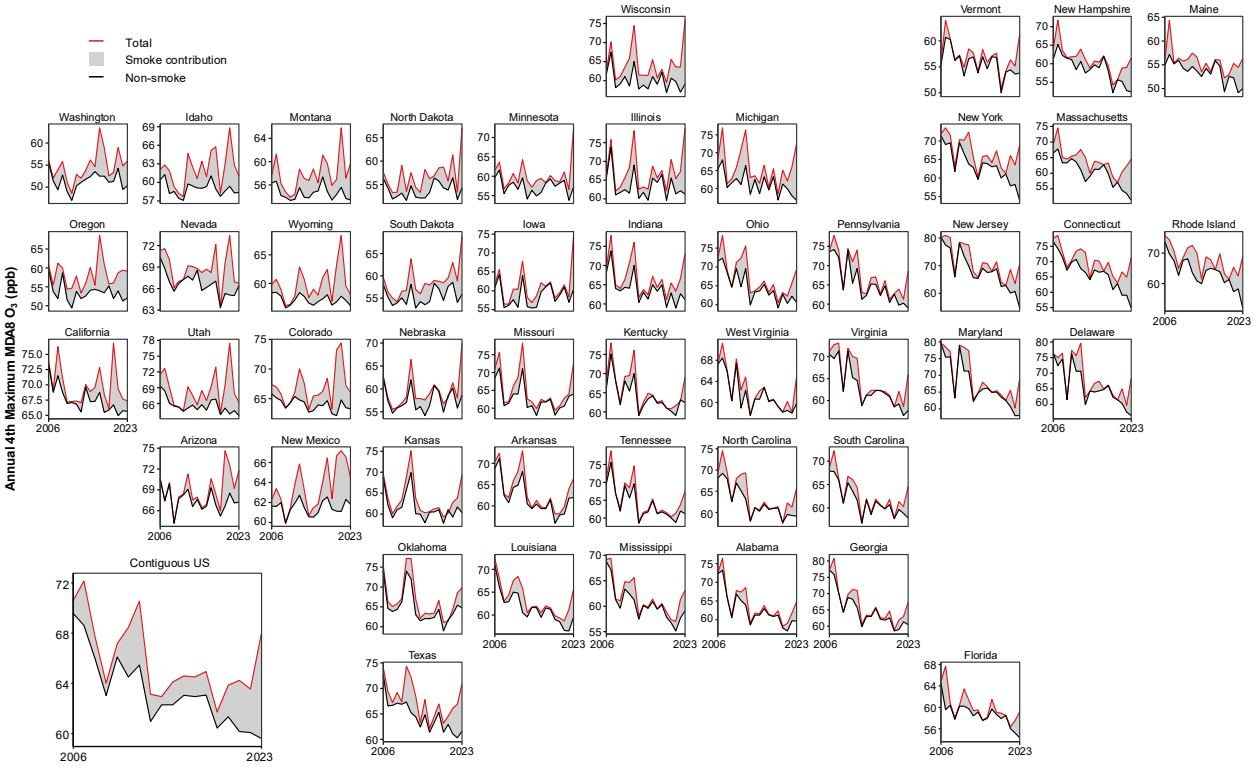


Figure 3: **The influence of wildfire smoke on population-weighted annual 4th-highest MDA8 $O_3$ across U.S. states.** Lines show annual population-weighted 4th-highest MDA8 $O_3$ for predicted total $O_3$ (red) and counterfactual non-smoke $O_3$ (black). Gray shading shows the smoke contribution, calculated by subtracting non-smoke $O_3$ from total $O_3$.

## Relationship between smoke $PM_{2.5}$ and smoke $O_3$

We found a non-linear and spatially heterogeneous relationship between smoke $PM_{2.5}$ and smoke $O_3$ across the contiguous U.S. (Figure 4). At the national level, daily smoke $O_3$ increases with smoke $PM_{2.5}$ up to a tipping point of approximately 60–70 $\mu g/m^3$ of daily smoke $PM_{2.5}$, beyond which smoke $O_3$ declines with further increases in smoke $PM_{2.5}$. This inverted U-shaped pattern is consistent with the documented effects that high smoke aerosol loading can suppress photochemical $O_3$ production by reducing light transmission and increasing $HO_2$ uptake, though existing evidence is mostly in the western U.S. (*28*, *49*). However, not all regions exhibit this pattern. In the Upper Midwest, Ohio Valley, South, and Southeast, smoke $O_3$ increases consistently with smoke $PM_{2.5}$ across the range of historically observed concentrations, with no evidence of a tipping point within observed levels. Even among regions that do exhibit an inverted U-shape, the tipping point varies substantially. We note that the spread of smoke $O_3$ within each smoke $PM_{2.5}$ bin is large (Figure

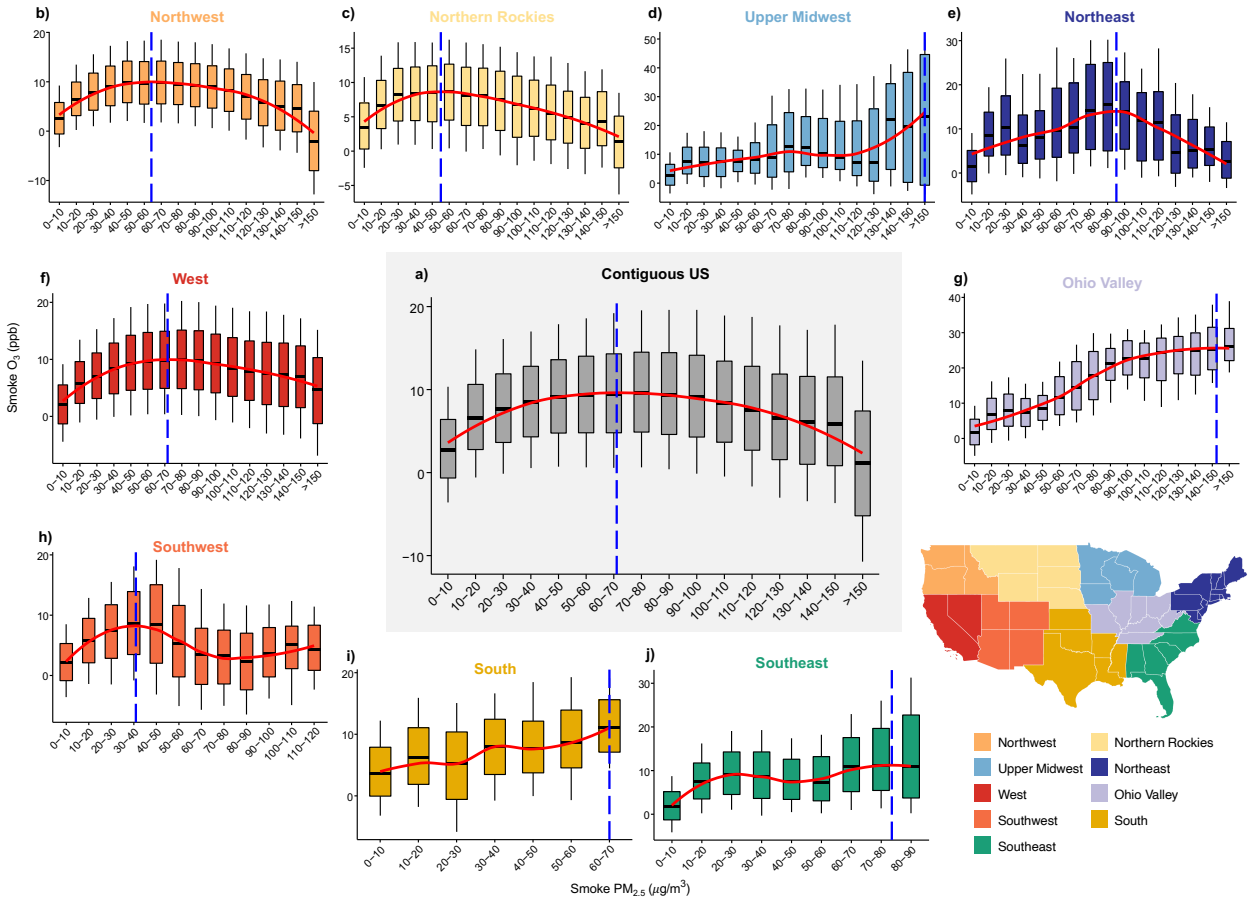


Figure 4: **National and regional patterns of non-linear relationships between smoke $PM_{2.5}$ and smoke $O_3$.** The boxplots illustrate the distributions of daily smoke $O_3$ within each daily smoke $PM_{2.5}$ bin: thick black lines represent the medians, box edges denote the 25th and 75th percentiles, and whiskers extend to the 10th and 90th percentiles. The solid red lines represent a LOESS regression fitted to the medians of each box. The vertical dashed blue lines indicate the smoke $PM_{2.5}$ threshold at which smoke $O_3$ concentrations reach their maximum value.

4), indicating that smoke $PM_{2.5}$ alone explains only a small fraction of the variation in smoke $O_3$. Overall, smoke $PM_{2.5}$ and smoke $O_3$ are only weakly correlated (with varying correlations across different smoke $PM_{2.5}$ ranges; Figure S15), suggesting that high smoke $PM_{2.5}$ exposure does not reliably predict high smoke $O_3$ exposure.

Smoke $O_3$ affected nearly all populations across the contiguous U.S., but meaningful differences in exposure exist across racial, ethnic, and income groups (Figure 5). For smoke $O_3$ exposures, Black populations face the highest exposure nationally (0.39–0.44 ppb across income deciles), followed by White (0.39–0.41 ppb), Hispanic (0.36–0.41 ppb), and Asian populations (0.33–0.37 ppb). A weak income gradient is present for most groups, with lower-income populations facing slightly higher

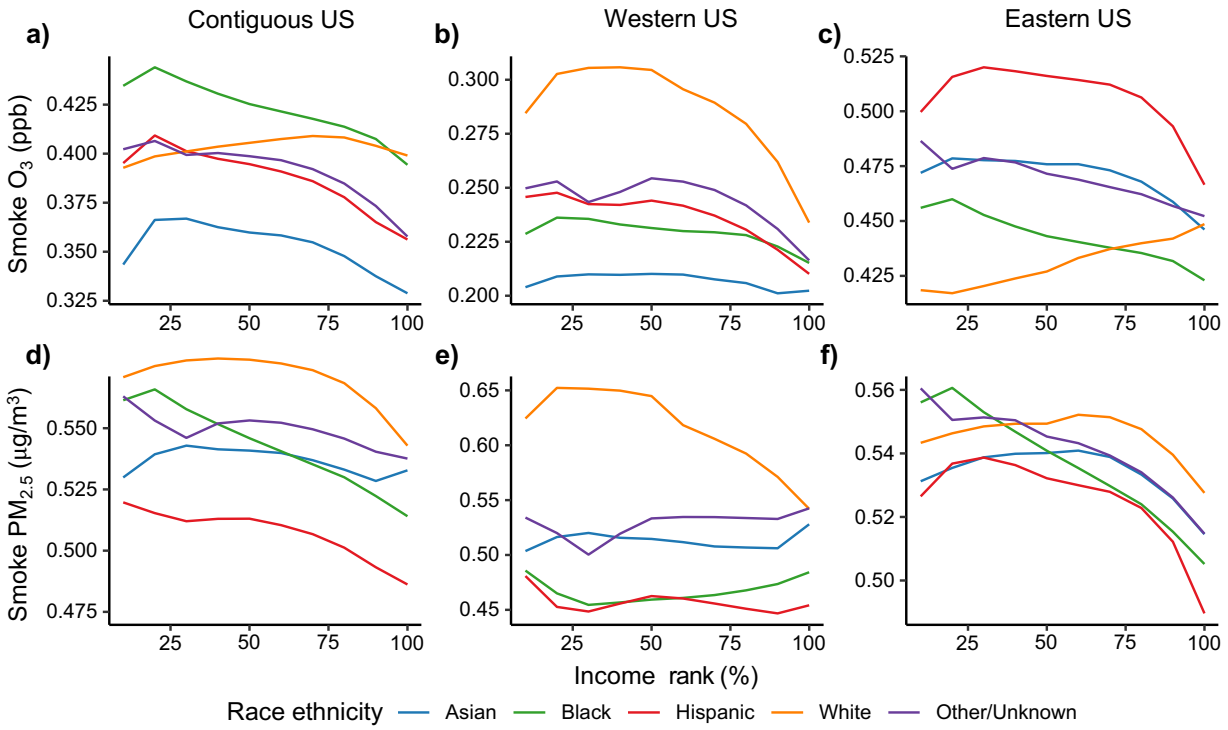


Figure 5: **Disparities in smoke $O_3$ and smoke $PM_{2.5}$ exposure by race/ethnicity and income groups.** Panels **a**–**c** show the average exposure to smoke $O_3$ across income rank (0–100%) and race or ethnicity (Asian, Black, Hispanic, White, and Other/Unknown) for the contiguous U.S., western U.S., and eastern U.S. The western U.S. is defined as locations west of the meridian 100° west. Panels **d**–**f** illustrate the corresponding exposure to smoke $PM_{2.5}$ for the same geographic regions.

smoke $O_3$ exposure. White populations are an exception and their smoke $O_3$ exposure is largely flat across income deciles. These distributional results differ from smoke $PM_{2.5}$ patterns, where White populations face the highest exposure (0.53–0.57 $\mu g/m^3$) and Hispanic populations face the lowest (0.47–0.51 $\mu g/m^3$). These contrasting patterns are driven by the different spatial distributions of the two pollutants combined with the geographic distribution of racial and income groups (Figures S16 and S17). In the western U.S. (defined as locations west of the meridian 100° west), where smoke $PM_{2.5}$ is highest, White populations face the greatest exposure to both pollutants. In the eastern U.S., where smoke $O_3$ is larger, Hispanic populations face the highest smoke $O_3$ exposure (0.47–0.52 ppb), while racial differences in smoke $PM_{2.5}$ are smaller. Prior studies have documented that wildfire smoke $PM_{2.5}$ exposure disparities do not follow conventional environmental justice patterns observed for non-smoke pollution (*23*, *50*, *51*). Our results suggest that considering smoke $O_3$ alongside smoke $PM_{2.5}$ adds further complexity to smoke exposure disparities.

# Discussion

In this study, we quantify the important and increasing contribution of wildfire smoke to U.S. $O_3$ trends, population exposure, and the nonattainment of national air quality standards. We found that wildfire smoke $O_3$ offset the otherwise declining trend in $O_3$ exposure and nonattainment populations over the study period. Smoke $O_3$ enhancement was widespread across the contiguous U.S. in recent years, with the Midwest experiencing the largest increases; this additional $O_3$ burden affected populations across all income and racial groups. The gridded smoke $O_3$ dataset we developed fills an important gap in existing smoke exposure products, which have focused almost exclusively on smoke $PM_{2.5}$ (*20*, *23*, *38*, *39*). Our findings extend prior monitor-based estimates of smoke $O_3$ (*30–33*) by providing spatially complete coverage that captures smoke $O_3$ in areas without surface monitors. The dataset also complements existing gridded total $O_3$ products by separating the wildfire smoke contribution from background $O_3$ (*52*, *53*).

Wildfire smoke influences on surface $O_3$ levels are highly complex, and our new gridded dataset provides a basis for investigating the underlying drivers of smoke $O_3$ at large regional scales. For example, future research could examine how smoke's effect on surface $O_3$ varies with fire and fuel characteristics, plume age, and the underlying $O_3$ chemistry regime. In constructing the smoke $O_3$ dataset, we carefully control for meteorological variability between smoke and non-smoke days, given that prior studies have shown that differences in ambient temperature and UV radiation between smoke and non-smoke days can substantially affect surface $O_3$ estimates (*31*). We also note that our approach treats all meteorological differences between smoke and non-smoke days as confounding factors to be accounted for. However, intense smoke events can themselves modify local meteorological conditions such as surface temperature and boundary layer height (*54*, *55*), suggesting that some portion of what we attribute to meteorological variability may itself be smoke-driven. Disentangling the direct effects of smoke on $O_3$ from these indirect meteorological pathways remains a challenge.

Our results indicate that smoke $O_3$ represents a distinct exposure that may not be well captured by smoke $PM_{2.5}$ alone. Consistent with prior monitor-based studies (*28*, *31*), we find that smoke $O_3$ and smoke $PM_{2.5}$ exhibit a complex inverted U-shaped relationship at the national level. A novel finding is that this relationship is regionally heterogeneous. The smoke $PM_{2.5}$–$O_3$ relationship also varies with distance from fires (Figure S18), consistent with the fact that $O_3$ is a secondary pollutant whose formation depends on plume age and the local chemical environment (*26*, *27*). These results

suggest that health risk assessments for wildfire smoke would benefit from incorporating $O_3$, particularly in regions where the relationship between the two pollutants is weakest. Epidemiological studies using multi-pollutant smoke exposure data are needed to identify the additional health risks attributable to wildfire smoke $O_3$ and to characterize potential interactions between smoke $O_3$ and smoke $PM_{2.5}$ (*56*, *57*).

The smoke $O_3$ estimates could be improved in several ways. First, following prior literature, our analysis relies on HMS smoke plumes for smoke day classification, which carries known uncertainties in representing surface-level smoke influence (*30*, *42*, *58*). In sensitivity tests, we exclude HMS-identified smoke days when there is no significant increase in estimated surface smoke $PM_{2.5}$ (*23*). If we remove all days with estimated smoke $PM_{2.5}$ less than 1 $\mu g/m^3$ (which accounts for 22% of all smoke days), our estimated population exposure to smoke $O_3$ and the smoke-driven nonattainment populations only decrease by 2% (Figure S19). Thus, our estimated smoke contribution to $O_3$ exposure is largely robust to uncertainty in the smoke day identification. Second, simulations from CTMs could complement our ML approach by providing alternative smoke day identifications when satellite imagery is missing or uncertain during extreme smoke events. CTM simulations can also represent the non-linear $O_3$ chemistry regimes that our empirical models cannot directly capture (*41*). Third, incorporating additional fire-related variables such as fuel type and fire dynamics may help improve prediction performance, particularly in the western U.S. where our models perform less well. Synoptic weather patterns and fine-scale meteorological features such as sea breeze circulations could also be incorporated as predictors (*17*, *59*).

The wildfire smoke $O_3$ dataset we created, together with the accompanying non-smoke $O_3$ predictions, can support a range of research and policy analyses. The dataset enables multi-pollutant epidemiological studies of both long-term and short-term health effects of wildfire smoke (*34*, *60*). Our estimates of smoke-driven $O_3$ exceedance can inform policy discussions about exceptional events under the Clean Air Act (*19*, *61*). The dataset can also support research on smoke $O_3$ effects on agriculture and ecosystems (*62*) considering the known impacts of $O_3$ on plants. As wildfire smoke is projected to continue increasing under future climate change (*63–65*), these impacts are likely to grow substantially without adaptation policies to mitigate them. Using high-resolution datasets to map their local impacts is an important and necessary step to further design and evaluate the interventions and adaptation strategies.

# Materials and Methods

## Datasets

For surface $O_3$ observations, we obtained daily maximum 8-hour average ozone (MDA8 $O_3$) across monitoring stations from the U.S. Environmental Protection Agency's (EPA) AirData repository (*66*). We used a variety of public datasets for smoke and fire information. We used smoke plume polygons generated from the National Oceanic and Atmospheric Administration (NOAA) Hazard Mapping System (HMS) from 2006 to 2023. Smoke polygons are generated daily using near-real-time visible satellite imagery to delineate the spatial distribution of wildfire smoke over the contiguous U.S. (*67*, *68*). We used gridded daily wildfire smoke $PM_{2.5}$ estimates for the contiguous U.S. at 10 km resolution from 2006 to 2023 from Childs et al. (*19*, *23*). Childs et al. constructed XGBoost models using satellite-derived smoke plume, remotely sensed atmospheric variables, interpolations of $PM_{2.5}$ measurements from surface monitors, meteorological variables, and fire variables to predict anomalous increases in surface $PM_{2.5}$ during wildfire events. For fire information, we used the Moderate Resolution Imaging Spectroradiometer (MODIS) Active Fire products (Collection 6) from 2006 to 2023 across the U.S. to identify fire point locations and fire radiative power (FRP) (*69*), as provided by NASA's Fire Information for Resource Management System (FIRMS) (*70*). Fire pixels within a 20 km radius are aggregated into a single fire event, with the event center computed as the weighted mean of the fire pixel locations based on FRP (*71*, *72*).

Surface nitrogen dioxide ($NO_2$) and formaldehyde (HCHO) data from a global reanalysis product are used as indicators of $O_3$ precursors. The Copernicus Atmosphere Monitoring Service (CAMS) Global Reanalysis, known as EAC4, is a comprehensive dataset of atmospheric composition produced by the European Centre for Medium-Range Weather Forecasts (ECMWF). It integrates a wide array of satellite observations with atmospheric modeling through data assimilation, providing consistent, three-dimensional global fields of various atmospheric constituents (*73*). The EAC4 product, available since 2003, provides global atmospheric data at a spatial resolution of 0.75 degree and a temporal resolution of 3 hours.

Meteorological data are sourced from both ERA5 and ERA5-Land products (*74*, *75*). We used daily ERA5-Land meteorological variables from 2006-2023 with a spatial resolution of 9 km, including 2m air temperature and dewpoint temperature (daily minimum, maximum, and mean), surface pressure, 10m v-component and u-component of wind, precipitation, surface (0-7cm) soil

moisture, and leaf area index (high and low vegetation). Mean sea level pressure, surface downward UV radiation, cloud cover, column ozone, and boundary layer height are derived from ERA5 with a spatial resolution of 25 km. We used elevation data from EarthEnv, a 1 km digital elevation model synthesized from global terrain data (*76*). Land cover classification is derived from the MODIS MCD12C1 product, which categorizes the global surface into 17 distinct types defined by the International Geosphere-Biosphere Programme at 0.05 degree resolution (*77*). Population data are derived from the Gridded Environmental Impacts Frame (Gridded EIF) developed by the U.S. Census Bureau and released in February 2025. The dataset includes detailed demographic counts by age, sex, race, ethnicity, and household income decile on a fixed 0.01-degree grid in North America (*78*).

**Smoke and non-smoke ML models**

To estimate smoke contribution to surface $O_3$ concentrations, we developed two sets of ML models – referred to as "smoke models" and "non-smoke models" to predict daily MDA8 $O_3$ concentration (Figure 1). Observational samples are classified into smoke and non-smoke datasets, based on the presence of HMS smoke plumes following prior methods (*23*, *30*, *32*). The smoke models use input variables from five categories: meteorological variables, $O_3$ precursor variables, geographical variables, fire-related variables, and interpolated $O_3$ concentrations from monitored data. The non-smoke models use all input features above except for fire-related variables and interpolated $O_3$ concentrations. A comprehensive list of features used in model training is provided in Table S3.

We constructed separate smoke and non-smoke ML models using three algorithms: eXtreme Gradient Boosting (XGBoost) (*79*), Categorical Boosting (CatBoost) (*80*), and Neural Network (NN) (*81*). To further enhance the predictive accuracy and robustness of our $O_3$ estimations, we implemented a stacking ensemble approach (*52*). This method integrates outputs of the three individual ML models by using their predictions as input features for a meta-learner. Specifically, we employed a Random Forest algorithm as the meta-learner to capture complex, non-linear relationships among the base model predictions. By combining multiple base learners, the ensemble model mitigates the biases inherent in individual models and leverages their complementary strengths, leading to improved generalization performance.

ML models' hyperparameters are tuned via 5-fold cross-validation (CV), using regression with Root Mean Squared Error (RMSE) as the objective function. Note that we construct two versions of the smoke models: one incorporating all variables, including interpolated $O_3$ concentrations from

EPA stations, and another excluding the interpolated $O_3$ concentrations. Here, the interpolated $O_3$ is calculated using inverse-distance weighting (IDW) spatial interpolation, based on ground-level $O_3$ observations from EPA monitoring stations. For each smoke day and each grid cell, we interpolate $O_3$ using all available monitor observations (*19*).

## Model Evaluations

We evaluated the model performance using 5-fold spatial CV. To address the concerns of information leakage between the training and test sets, we split data by station locations, rather than using a conventional random split by observation (where a given station could contribute data to both sets). The spatial folds (disjoint sets of training and testing) are defined from the coarsest input (CAMS, $\sim$75 km) to avoid further information leakages. Model performance is also assessed with a spatial split at 150 km to quantify its performance in regions with sparse monitor coverage. As discussed in prior literature, spatial CV provides a more realistic assessment of the model's ability to predict MDA8 $O_3$ at new locations with no surface observations (*23*, *82*). We reported four evaluation metrics: $R^2$, within $R^2$, RMSE, and Mean Absolute Error (MAE) on the held-out test set. Within $R^2$ is calculated by regressing observed MDA8 $O_3$ on predicted MDA8 $O_3$, including fixed effects for each station and month, thereby isolating within-location temporal variation. We employed SHapley Additive exPlanations (SHAP) (*83*) to enhance the interpretability of our ML models and understand the contribution of each feature to the predicted MDA8 $O_3$ concentrations (Figures S6 and S7).

## Predicting smoke $O_3$

To generate grid-level smoke $O_3$ estimates, we used our smoke and non-smoke models to predict $O_3$ on each smoke day and non-smoke day from 2006-2023 across all grid cells (10 km) in the contiguous U.S. For non-smoke days, we used the non-smoke models to predict $O_3$ concentrations on those days across contiguous U.S. These predictions on non-smoke days use feature values observed on that day, e.g., meteorology and precursor concentration, and are thus designed to represent the actual $O_3$ concentration on those days. For smoke days, we used our ML models to create three sets of predictions (Figure 1):

- *Predicted total* $O_3 = f_S(M, P, G, F)$, where $f_S$ represents the smoke ML models, and M,P,G,F represent the input features of meteorology variables (M), precursor variables (P), geographical

variables (G), and fire-related variables (F). *Predicted total* $O_3$ is predicted from the smoke model, using meteorological and precursor variables observed on the corresponding smoke day. *Predicted total* $O_3$ thus estimates the total $O_3$ concentration from both smoke and non-smoke sources on smoke days.

- *Counterfactual* $O_3 = f_{NS}(M, \overline{P_{NS}}, G)$, where $f_{NS}$ represents the non-smoke ML models, and $\overline{P_{NS}}$ represents the values of precursor variables averaged over non-smoke days in the same month with 3-year windows. Note that *Counterfactual* $O_3$ is predicted from the non-smoke models using meteorological variables observed on the corresponding smoke day and average precursor values on non-smoke days. *Counterfactual* $O_3$ thus estimates the counterfactual non-smoke $O_3$ concentration on smoke days given the observed meteorological conditions.

- *Non-Smoke met* $O_3 = f_{NS}(\overline{M}, \overline{P_{NS}}, G)$, where $f_{NS}$ represents the non-smoke ML models, $\overline{M}$ represents the average meteorological conditions over non-smoke days, and $\overline{P_{NS}}$ represents the average precursor variables over non-smoke days. Note that *Non-Smoke met* $O_3$ is predicted from the non-smoke model using average meteorological and precursor variable values on non-smoke days. *Non-Smoke met* $O_3$ thus quantifies the counterfactual non-smoke $O_3$ concentration on smoke days given the typical non-smoke meteorological conditions for this grid cell. Non-smoke meteorological conditions are defined as the mean values of meteorological variables on all non-smoke days in the same month and the moving 3-year window.

We then used these three sets of predictions on smoke days to estimate the contribution of wildfire smoke on ground-level $O_3$ concentrations and the contribution of meteorological variability between smoke and non-smoke days on $O_3$ concentrations. Specifically, we calculated two values for each smoke day:

$$\text{Smoke-driven } O_3 = \textit{Predicted total } O_3 - \textit{Counterfactual } O_3 \tag{1}$$

$$\text{Met-driven } O_3 = \textit{Counterfactual } O_3 - \textit{Non-Smoke met } O_3 \tag{2}$$

Here, *Smoke-driven* $O_3$ denotes the contribution of wildfire smoke to ground-level $O_3$ concentrations while controlling for meteorological variability between smoke and non-smoke days. Importantly, *Smoke-driven* $O_3$ does not include the potential $O_3$ changes due to meteorological variability across smoke and non-smoke days (e.g., smoke days are hotter). We use *Smoke-driven* $O_3$ as our

main estimates for smoke $O_3$ concentration. *Met-driven $O_3$* quantifies the effects of meteorological variability on $O_3$ concentrations, which is not necessarily due to smoke influences. We retain all values of *Smoke-driven $O_3$* and *Met-driven $O_3$*, whether positive or negative, in all calculations. *Smoke-driven $O_3$* are assumed to be zero on non-smoke days.

Our final dataset thus includes 1.72 million daily grid-cell smoke-day observations across 95,549 grid cells from 2006-2023 (grid cells with water coverage >50% are excluded). As we construct two versions of the smoke model, one with and one without interpolated $O_3$ concentrations, we generate two sets of predicted total $O_3$ concentrations and estimated *Smoke-driven $O_3$* for all smoke days. We do not construct non-smoke models with interpolated $O_3$ concentrations because our non-smoke models already perform adequately even without interpolations. As a result, our final model only includes one set of predicted total $O_3$ concentrations for all non-smoke days, and one set of predictions for *Met-driven $O_3$* on smoke days.

## Acknowledgments

M.Q. acknowledged the support from Minghua Zhang faculty career catalyst award from Stony Brook University. X.J. acknowledged the support from NOAA Climate Program Office's Atmospheric Chemistry, Carbon Cycle, and Climate program (grant number: NA22OAR4310199). K.C. was supported by the National Heart, Lung, and Blood Institute of the National Institutes of Health (R01HL169171). Role of the Funder/Sponsor: The funder had no role in the design and conduct of the study; collection, management, analysis, and interpretation of the data; preparation, review, or approval of the manuscript; and decision to submit the manuscript for publication.


## Author contributions

M.Q. designed the research. Y.L. led the development of machine learning models, with inputs from M.C., M.K., X.J., and K.C. M.Q. and Y.L. led the analysis on smoke ozone exposure patterns, with inputs from all co-authors. M.Q. and Y.L. drafted the manuscript with inputs from all co-authors. All authors reviewed and approved the manuscript.

## Competing interests

The authors declare no competing interests.

## Data and materials availability

Generated daily smoke $O_3$ data can be downloaded at https://doi.org/10.5281/zenodo.20346286. Replication data and materials to produce the main results and figures of the paper are available at https://github.com/mhqiu/US-smoke-ozone.

# References


1. U.S. Environmental Protection Agency, *Green Book: Nonattainment Areas for Criteria Pollutants*, Accessed: 2026-05-18, 2026.

2. J. Zhang, Y. Wei, Z. Fang, Ozone pollution: a major health hazard worldwide. *Frontiers in immunology* **10**, 2518 (2019).

3. Y. You *et al.*, Impact of Short-Term Exposure to Ozone on Hospital Admissions for Multiple Cardiovascular Diseases: A Systematic Review and Meta-Analysis. *Journal of the American Heart Association* **14**, e037205 (2025).

4. L. Chu *et al.*, Joint exposure to Ozone and temperature and acute myocardial infarction among adults aged 18 to 64 years in the united States. *Circulation* **152**, 246–256 (2025).

5. Q. Di *et al.*, Air pollution and mortality in the Medicare population. *New England Journal of Medicine* **376**, 2513–2522 (2017).

6. H. Z. Sun *et al.*, Cohort-based long-term ozone exposure-associated mortality risks with adjusted metrics: a systematic review and meta-analysis. *The Innovation* **3** (2022).

7. O. R. Cooper, R.-S. Gao, D. Tarasick, T. Leblanc, C. Sweeney, Long-term ozone trends at rural ozone monitoring sites across the United States, 1990–2010. *Journal of Geophysical Research: Atmospheres* **117**, D22307 (2012).

8. H. Simon, A. Reff, B. Wells, J. Xing, N. Frank, Ozone trends across the United States over a period of decreasing NOx and VOC emissions. *Environmental science & technology* **49**, 186–195 (2015).

9. I. C. Dedoussi, S. D. Eastham, E. Monier, S. R. Barrett, Premature mortality related to United States cross-state air pollution. *Nature* **578**, 261–265 (2020).

10. M. Lin, L. W. Horowitz, R. Payton, A. M. Fiore, G. Tonnesen, US surface ozone trends and extremes from 1980 to 2014: quantifying the roles of rising Asian emissions, domestic controls, wildfires, and climate. *Atmospheric Chemistry and Physics* **17**, 2943–2970 (2017).

11. H. He, X.-Z. Liang, C. Sun, Z. Tao, D. Q. Tong, The long-term trend and production sensitivity change in the US ozone pollution from observations and model simulations. *Atmospheric Chemistry and Physics* **20**, 3191–3208 (2020).

*12.* T. Ansari *et al.*, Explaining trends and changing seasonal cycles of surface ozone in North America and Europe over the 2000–2018 period: a global modelling study with NO x and VOC tagging. *Atmospheric Chemistry and Physics* **25**, 16833–16876 (2025).

*13.* K.-L. Chang, B. C. McDonald, C. Harkins, O. R. Cooper, Surface ozone trend variability across the United States and the impact of heat waves (1990–2023). *Atmospheric Chemistry and Physics* **25**, 5101–5132 (2025).

*14.* D. A. Jaffe, M. Ninneman, H. C. Chan, NOx and O3 trends at U.S. non-attainment areas for 1995–2020: Influence of COVID-19 reductions and wildland fires on policy-relevant concentrations. *Journal of Geophysical Research: Atmospheres* **127**, e2021JD036385 (2022).

*15.* Z. Jiang *et al.*, Unexpected slowdown of US pollutant emission reduction in the past decade. *Proceedings of the National Academy of Sciences* **115**, 5099–5104 (2018).

*16.* M. M. Coggon *et al.*, Volatile chemical product emissions enhance ozone and modulate urban chemistry. *Proceedings of the National Academy of Sciences* **118**, e2026653118 (2021).

*17.* D. A. Jaffe *et al.*, Scientific assessment of background ozone over the U.S.: Implications for air quality management. *Elementa: Science of the Anthropocene* **6**, 56 (2018).

*18.* V. Iglesias, J. K. Balch, W. R. Travis, US fires became larger, more frequent, and more widespread in the 2000s. *Science Advances* **8**, eabc0020 (2022).

*19.* M. Childs *et al.*, Growing wildfire-derived PM2. 5 across the contiguous US and implications for air quality regulation. (2024).

*20.* D. Zhang *et al.*, Wildland Fires Worsened Population Exposure to PM2. 5 Pollution in the Contiguous United States. *Environmental Science & Technology* **57**, 19990–19998 (2023).

*21.* C. D. McClure, D. A. Jaffe, US particulate matter air quality improves except in wildfire-prone areas. *Proceedings of the National Academy of Sciences* **115**, 7901–7906 (2018).

*22.* M. Burke *et al.*, The contribution of wildfire to PM2. 5 trends in the USA. *Nature* **622**, 761–766 (2023).

*23.* M. L. Childs *et al.*, Daily Local-Level Estimates of Ambient Wildfire Smoke PM2. 5 for the Contiguous US. *Environmental Science & Technology* **56**, 13607–13621 (2022).

*24.* D. Jaffe, H. Lee, S. Magzamen, D. L. Goldberg, K. O'Dell, Health and regulatory impacts of PM2. 5 from wildland fires for 2019–2024 in the US. *GeoHealth* **10**, e2025GH001576 (2026).

445 *25.* D. A. Jaffe, N. L. Wigder, Ozone production from wildfires: A critical review. *Atmospheric*
446 *Environment* **51**, 1–10 (2012).

447 *26.* D. A. Jaffe *et al.*, Wildfire and prescribed burning impacts on air quality in the United States.
448 *Journal of the Air & Waste Management Association* **70**, 583–615 (2020).

449 *27.* L. Xu *et al.*, Ozone chemistry in western US wildfire plumes. *Science Advances* **7**, eabl3648
450 (2021).

451 *28.* J. Shen, R. C. Cohen, G. M. Wolfe, X. Jin, Impacts of wildfire smoke aerosols on near-surface
452 ozone photochemistry. *Atmospheric Chemistry and Physics* **25**, 8701–8718 (2025).

453 *29.* J. O. Palmo *et al.*, Investigating fire-induced ozone production from local to global scales.
454 *Atmospheric Chemistry and Physics* **25**, 17107–17124 (2025).

455 *30.* H. Lee, D. A. Jaffe, Wildfire impacts on O3 in the continental United States using PM2. 5 and
456 a generalized additive model (2018–2023). *Environmental Science & Technology* **58**, 14764–
457 14774 (2024).

458 *31.* Y. Li, X. Jin, M. Kelp, H. Z. Sun, M. Qiu, Growing impacts of fire smoke on ozone pollution
459 and associated mortality burden in the United States. *Science Advances* **12**, eaec2903 (2026).

460 *32.* S. J. Brey, E. V. Fischer, Smoke in the city: How often and where does smoke impact summer-
461 time ozone in the United States? *Environmental Science & Technology* **50**, 1288–1294 (2016).

462 *33.* H. Lee, D. A. Jaffe, Impact of wildfires on O3 and air quality across the United States for
463 2019–2024 using generalized additive models. *Journal of Geophysical Research: Atmospheres*
464 **130**, e2025JD044088 (2025).

465 *34.* R. Aguilera, T. Benmarhnia, Effects of Multiple Wildfire Smoke Pollutants ($PM_{2.5}$, $PM_{10}$,
466 and Ozone) on Respiratory and Cardiovascular Hospitalizations in California (2006–2019).
467 *GeoHealth* (2025).

468 *35.* L. Jin *et al.*, Characterizing emissions, chemistry, and health impacts of aged wildfire smoke
469 in a western US city. *EGUsphere*, Preprint (2026).

470 *36.* K. O'Dell, B. Ford, E. V. Fischer, J. R. Pierce, Contribution of wildland-fire smoke to US
471 PM2. 5 and its influence on recent trends. *Environmental Science & Technology* **53**, 1797–
472 1804 (2019).

*37.* S. N. Koplitz, C. G. Nolte, G. A. Pouliot, J. M. Vukovich, J. Beidler, Influence of uncertainties in burned area estimates on modeled wildland fire $PM_{2.5}$ and ozone pollution in the contiguous U.S. *Atmospheric Environment* **191**, 328–339 (2018).

*38.* R. Aguilera *et al.*, A novel ensemble-based statistical approach to estimate daily wildfire-specific PM2. 5 in California (2006–2020). *Environment International* **171**, 107719 (2023).

*39.* Y. Hu *et al.*, Global high-resolution fire-sourced $PM_{2.5}$ concentrations for 2000–2023. *Earth System Science Data* **17**, 3741–3756 (2025).

*40.* T. S. Carter *et al.*, How emissions uncertainty influences the distribution and radiative impacts of smoke from fires in North America. *Atmospheric Chemistry and Physics* **20**, 2073–2097 (2020).

*41.* L. Jin *et al.*, Ozone photochemistry in fresh biomass burning smoke over the United States. *Science Advances* **12**, eads2157 (2026).

*42.* M. Qiu *et al.*, Evaluating Chemical Transport and Machine Learning Models for Wildfire Smoke PM2. 5: Implications for Assessment of Health Impacts. *Environmental Science & Technology* **58**, 22880–22893 (2024).

*43.* M. Lin *et al.*, Springtime high surface ozone events over the western United States: Quantifying the role of stratospheric intrusions. *Journal of Geophysical Research: Atmospheres* **117** (2012).

*44.* Q. Zhu *et al.*, A better representation of volatile organic compound chemistry in WRF-Chem and its impact on ozone over Los Angeles. *Atmospheric chemistry and physics* **24**, 5265–5286 (2024).

*45.* O. R. Cooper *et al.*, Early season 2023 wildfires generated record-breaking surface ozone anomalies across the US Upper Midwest. *Geophysical Research Letters* **51**, e2024GL111481 (2024).

*46.* M. Lin, L. W. Horowitz, L. Hu, W. Permar, Reactive Nitrogen Partitioning Enhances the Contribution of Canadian Wildfire Plumes to US Ozone Air Quality. *Geophysical Research Letters* **51** (2024).

*47.* W. S. Chace *et al.*, The Influence of Aged Smoke on Urban Ozone: Aircraft Measurements in Chicago during the 2023 Canadian Wildfires. (2026).

*48.* M. Ninneman, D. A. Jaffe, The impact of wildfire smoke on ozone production in an urban area: Insights from field observations and photochemical box modeling. *Atmospheric Environment* **267**, 118764 (2021).

*49.* X. Jiang, C. Wiedinmyer, A. G. Carlton, Aerosols from fires: An examination of the effects on ozone photochemistry in the Western United States. *Environmental Science & Technology* **46**, 11878–11886 (2012).

*50.* J. A. Casey *et al.*, Measuring long-term exposure to wildfire PM2.5 in California: Time-varying inequities in environmental burden. *Proceedings of the National Academy of Sciences* **121**, e2306729121 (2024).

*51.* L. R. Dennin, D. Nock, N. Z. Muller, M. Akindele, P. J. Adams, Socially vulnerable communities face disproportionate exposure and susceptibility to U.S. wildfire and prescribed burn smoke. *Communications Earth & Environment* **6**, 190 (2025).

*52.* W. J. Requia *et al.*, An ensemble learning approach for estimating high spatiotemporal resolution of ground-level ozone in the contiguous United States. *Environmental science & technology* **54**, 11037–11047 (2020).

*53.* J. Wang *et al.*, Fire-Driven Trend Reversal in U.S. Ozone Exposure and Air Quality Progress. *Research Square*, Preprint, under review at Nature Portfolio (2025).

*54.* X. Huang *et al.*, Smoke-weather interaction affects extreme wildfires in diverse coastal regions. *Science* **379**, 457–461 (2023).

*55.* G. A. Kelesidis *et al.*, Radiative cooling in New York/New Jersey metropolitan areas by wildfire particulate matter emitted from the Canadian wildfires of 2023. *Communications Earth & Environment* **6**, 304 (2025).

*56.* C. Liu *et al.*, Interactive effects of ambient fine particulate matter and ozone on daily mortality in 372 cities: two stage time series analysis. *bmj* **383** (2023).

*57.* N. Siddika *et al.*, Synergistic effects of prenatal exposure to fine particulate matter (PM2. 5) and ozone (O3) on the risk of preterm birth: A population-based cohort study. *Environmental research* **176**, 108549 (2019).

*58.* T. Liu *et al.*, Is the smoke aloft? Caveats regarding the use of the Hazard Mapping System (HMS) smoke product as a proxy for surface smoke presence across the United States. *International Journal of Wildland Fire* **33** (2024).

*59.* L Shen, L. Mickley, A. Tai, Influence of synoptic patterns on surface ozone variability over the eastern United States from 1980 to 2012. *Atmospheric Chemistry and Physics* **15**, 10925–10938 (2015).

60. S. Heft-Neal *et al.*, Emergency department visits respond nonlinearly to wildfire smoke. *Proceedings of the National Academy of Sciences* **120**, e2302409120 (2023).

61. A. Krupnick, N. Richardson, M. Wibbenmeyer, Wildfire Smoke, the Clean Air Act, and the Exceptional Events Rule: Implications and Policy Alternatives. *Environmental Science & Technology* **59**, 2917–2927 (2025).

62. L. Emberson, Effects of ozone on agriculture, forests and grasslands. *Philosophical Transactions of the Royal Society A* **378**, 20190327 (2020).

63. M. Qiu *et al.*, Wildfire smoke exposure and mortality burden in the USA under climate change. *Nature* **647**, 935–943 (2025).

64. M. Qiu *et al.*, Valuing wildfire smoke–related mortality benefits from climate mitigation. *Proceedings of the National Academy of Sciences* **123**, e2533772123 (2026).

65. Y. Xie *et al.*, Tripling of western US particulate pollution from wildfires in a warming climate. *Proceedings of the National Academy of Sciences* **119**, e2111372119 (2022).

66. U.S EPA, "Overview of Ozone (O3) Air Quality in the United States", tech. rep.

67. W Schroeder *et al.*, Validation analyses of an operational fire monitoring product: The Hazard Mapping System. *International Journal of Remote Sensing* **29**, 6059–6066 (2008).

68. M. Ruminski, S. Kondragunta, R. Draxler, J. Zeng, presented at the Proceedings of the 15th International Emission Inventory Conference, vol. 15, p. 18.

69. L. Giglio, W. Schroeder, C. O. Justice, The collection 6 MODIS active fire detection algorithm and fire products. *Remote Sensing of Environment* **178**, 31–41 (2016).

70. D. Davies *et al.*, presented at the EARSel Forest Fires SIG Workshop.

71. X. Jin, Q. Zhu, R. C. Cohen, Direct estimates of biomass burning NO x emissions and lifetimes using daily observations from TROPOMI. *Atmospheric Chemistry and Physics* **21**, 15569–15587 (2021).

72. X. Jin, A. M. Fiore, R. C. Cohen, Space-based observations of ozone precursors within California wildfire plumes and the impacts on ozone-NO x-VOC chemistry. *Environmental Science & Technology* **57**, 14648–14660 (2023).

73. A. Inness *et al.*, The CAMS reanalysis of atmospheric composition. *Atmospheric Chemistry and Physics* **19**, 3515–3556 (2019).

562 *74.* H. Hersbach *et al.*, The ERA5 global reanalysis. *Quarterly Journal of the Royal Meteorological*
563 *Society* **146**, 1999–2049 (2020).

564 *75.* J. Muñoz Sabater *et al.*, ERA5-Land: a state-of-the-art global reanalysis dataset for land
565 applications. *Earth System Science Data* **13**, 4349–4383 (2021).

566 *76.* G. Amatulli *et al.*, A suite of global, cross-scale topographic variables for environmental and
567 biodiversity modeling. *Scientific Data* **5**, 1–15 (2018).

568 *77.* D. Sulla-Menashe, M. A. Friedl, *et al.*, User guide to collection 6 MODIS land cover (MCD12Q1
569 and MCD12C1) product. *Usgs: Reston, Va, Usa* **1**, 18 (2018).

570 *78.* J. Voorheis *et al.*, "The Privacy-Protected Gridded Environmental Impacts Frame", Working
571 Papers 24-74 (Center for Economic Studies, U.S. Census Bureau, Dec. 2024).

572 *79.* T. Chen, C. Guestrin, presented at the Proceedings of the 22nd ACM SIGKDD International
573 Conference on Knowledge Discovery and Data Mining, pp. 785–794.

574 *80.* L. Prokhorenkova, G. Gusev, A. Vorobev, A. V. Dorogush, A. Gulin, CatBoost: unbiased boost-
575 ing with categorical features. *Advances in neural information processing systems* **31** (2018).

576 *81.* R. Miikkulainen *et al.*, in *Artificial intelligence in the age of neural networks and brain com-*
577 *puting* (Elsevier, 2024), pp. 269–287.

578 *82.* A. van Donkelaar *et al.*, North American Fine Particulate Matter Chemical Composition for
579 2000–2022 from Satellites, Models, and Monitors: The Changing Contribution of Wildfires.
580 *ACS ES&T Air* **1**, 1589–1600 (2024).

581 *83.* S. M. Lundberg, S.-I. Lee, A unified approach to interpreting model predictions. *Advances in*
582 *neural information processing systems* **30** (2017).

Table S1: Out-of-sample performance metrics of smoke and non-smoke $O_3$ models, reported based on spatial cross-validation at 75 km. Within $R^2$ is calculated from linear regressions that include station and month fixed effects, thus capturing the models' ability to capture spatio-temporal variability beyond seasonality and time-invariant location differences. Warm season is defined as April to September.

| **Model group** | **Learner** | $R^2$ | **Within** $R^2$ | **RMSE (ppb)** | **MAE (ppb)** |
|---|---|---|---|---|---|
| Non-smoke (all-year) | XGBoost | 0.73 | 0.58 | 7.23 | 5.42 |
| | CatBoost | 0.73 | 0.57 | 7.34 | 5.53 |
| | Neural Network | 0.69 | 0.52 | 7.74 | 5.85 |
| | Ensemble | 0.73 | 0.57 | 7.28 | 5.47 |
| Non-smoke (warm-season) | XGBoost | 0.69 | 0.56 | 7.94 | 5.99 |
| | CatBoost | 0.69 | 0.56 | 8.05 | 6.13 |
| | Neural Network | 0.65 | 0.51 | 8.46 | 6.47 |
| | Ensemble | 0.68 | 0.56 | 7.98 | 6.05 |
| Smoke (no interpolation) | XGBoost | 0.74 | 0.65 | 7.33 | 5.41 |
| | CatBoost | 0.72 | 0.62 | 7.75 | 5.83 |
| | Neural Network | 0.66 | 0.54 | 8.23 | 6.25 |
| | Ensemble | 0.73 | 0.64 | 7.39 | 5.50 |
| Smoke (with interpolation) | XGBoost | 0.86 | 0.81 | 5.61 | 3.96 |
| | CatBoost | 0.86 | 0.81 | 5.58 | 3.93 |
| | Neural Network | 0.85 | 0.80 | 5.79 | 4.11 |
| | Ensemble | 0.85 | 0.81 | 5.73 | 4.07 |

Table S2: Population-weighted annual 4th maximum MDA8 $O_3$ concentrations by state (unit: ppb). Three separate periods, 2006-2023, 2006-2008, and 2021-2023, are shown in the table.

| State | **Non-smoke $O_3$** | | | **Total $O_3$** | | | **Smoke Contribution** | | |
|---|---|---|---|---|---|---|---|---|---|
| | 2006–2023 | 2006–2008 | 2021–2023 | 2006–2023 | 2006–2008 | 2021–2023 | 2006–2023 | 2006–2008 | 2021–2023 |
| **contiguous U.S.** | 63.3 | 68.1 | 59.9 | 65.9 | 70.1 | 65.3 | 2.61 | 2.06 | 5.35 |
| Alabama | 62.8 | 70.5 | 58.9 | 64.1 | 71.7 | 61.8 | 1.32 | 1.20 | 2.95 |
| Arizona | 67.6 | 69.4 | 67.7 | 69.0 | 69.4 | 71.2 | 1.44 | 0.06 | 3.50 |
| Arkansas | 62.1 | 67.5 | 60.7 | 63.6 | 68.6 | 63.4 | 1.52 | 1.04 | 2.72 |
| California | 67.6 | 71.3 | 65.5 | 69.8 | 73.1 | 68.2 | 2.21 | 1.86 | 2.63 |
| Colorado | 64.0 | 65.2 | 63.9 | 67.0 | 66.8 | 69.3 | 2.96 | 1.56 | 5.40 |
| Connecticut | 66.2 | 74.1 | 57.8 | 70.1 | 76.5 | 67.6 | 3.88 | 2.45 | 9.87 |
| Delaware | 65.8 | 74.4 | 58.2 | 68.5 | 76.0 | 64.5 | 2.68 | 1.57 | 6.25 |
| Florida | 58.6 | 61.4 | 55.1 | 60.2 | 64.5 | 57.7 | 1.56 | 3.04 | 2.58 |
| Georgia | 65.0 | 74.4 | 60.4 | 66.6 | 76.2 | 64.1 | 1.62 | 1.74 | 3.64 |
| Idaho | 59.1 | 60.0 | 58.8 | 62.2 | 62.3 | 64.3 | 3.15 | 2.29 | 5.50 |
| Illinois | 63.6 | 66.9 | 61.7 | 67.5 | 68.1 | 70.6 | 3.88 | 1.14 | 8.90 |
| Indiana | 64.0 | 68.7 | 61.0 | 67.0 | 70.8 | 67.7 | 2.96 | 2.03 | 6.70 |
| Iowa | 58.9 | 60.3 | 59.5 | 61.3 | 61.4 | 65.0 | 2.40 | 1.12 | 5.46 |
| Kansas | 61.7 | 63.4 | 60.5 | 63.7 | 64.6 | 65.4 | 2.08 | 1.15 | 4.87 |
| Kentucky | 64.2 | 69.8 | 61.6 | 65.8 | 71.5 | 64.6 | 1.66 | 1.66 | 2.95 |
| Louisiana | 61.7 | 66.7 | 57.7 | 63.5 | 67.8 | 61.9 | 1.80 | 1.12 | 4.20 |
| Maine | 53.5 | 55.7 | 50.4 | 55.7 | 58.5 | 55.3 | 2.24 | 2.79 | 4.86 |
| Maryland | 67.2 | 77.0 | 59.0 | 69.4 | 78.5 | 65.0 | 2.19 | 1.52 | 6.01 |
| Massachusetts | 60.3 | 65.9 | 53.2 | 64.2 | 69.7 | 62.5 | 3.90 | 3.80 | 9.24 |
| Michigan | 61.5 | 64.7 | 58.3 | 66.0 | 68.9 | 67.0 | 4.57 | 4.22 | 8.66 |
| Minnesota | 57.6 | 59.1 | 56.8 | 60.4 | 60.8 | 63.5 | 2.80 | 1.68 | 6.72 |
| Mississippi | 60.5 | 65.8 | 57.4 | 61.8 | 66.7 | 60.4 | 1.33 | 0.91 | 3.07 |
| Missouri | 63.0 | 66.9 | 62.8 | 65.3 | 69.5 | 66.6 | 2.34 | 2.57 | 3.79 |
| Montana | 54.7 | 55.8 | 54.3 | 57.9 | 58.4 | 60.9 | 3.23 | 2.66 | 6.62 |
| Nebraska | 57.6 | 58.2 | 58.2 | 59.6 | 58.9 | 63.2 | 1.99 | 0.67 | 4.96 |
| Nevada | 66.7 | 68.7 | 65.5 | 68.8 | 71.0 | 69.1 | 2.11 | 2.27 | 3.54 |
| New Hampshire | 58.5 | 63.0 | 53.4 | 61.2 | 66.5 | 59.8 | 2.66 | 3.50 | 6.42 |

...

**Table S2**

| State | Non-smoke $O_3$ | | | Total $O_3$ | | | Smoke Contribution | | |
|---|---|---|---|---|---|---|---|---|---|
| | 2006–2023 | 2006–2008 | 2021–2023 | 2006–2023 | 2006–2008 | 2021–2023 | 2006–2023 | 2006–2008 | 2021–2023 |
| New Jersey | 68.3 | 78.1 | 58.7 | 71.6 | 80.6 | 67.7 | 3.34 | 2.45 | 9.04 |
| New Mexico | 61.5 | 61.8 | 61.8 | 63.6 | 62.7 | 66.1 | 2.07 | 0.94 | 4.36 |
| New York | 63.4 | 70.0 | 56.8 | 67.0 | 72.4 | 66.2 | 3.62 | 2.37 | 9.43 |
| North Carolina | 62.4 | 68.4 | 59.3 | 64.2 | 71.2 | 63.2 | 1.86 | 2.77 | 3.91 |
| North Dakota | 53.8 | 54.2 | 54.2 | 56.9 | 55.4 | 60.7 | 3.15 | 1.23 | 6.46 |
| Ohio | 64.8 | 70.8 | 61.1 | 67.4 | 73.4 | 65.9 | 2.63 | 2.51 | 4.79 |
| Oklahoma | 65.0 | 67.6 | 64.6 | 67.0 | 69.0 | 67.7 | 2.03 | 1.47 | 3.10 |
| Oregon | 53.7 | 55.2 | 52.6 | 58.3 | 59.3 | 59.2 | 4.65 | 4.08 | 6.62 |
| Pennsylvania | 65.4 | 73.4 | 59.8 | 67.5 | 75.2 | 64.6 | 2.10 | 1.82 | 4.79 |
| Rhode Island | 63.5 | 70.4 | 56.0 | 68.0 | 73.7 | 65.6 | 4.54 | 3.36 | 9.67 |
| South Carolina | 61.6 | 67.3 | 58.9 | 62.9 | 69.1 | 62.1 | 1.29 | 1.79 | 3.19 |
| South Dakota | 55.6 | 55.7 | 56.3 | 58.8 | 57.1 | 63.7 | 3.27 | 1.43 | 7.40 |
| Tennessee | 64.0 | 70.8 | 60.8 | 65.6 | 72.4 | 64.3 | 1.53 | 1.57 | 3.51 |
| Texas | 64.4 | 68.6 | 60.9 | 67.7 | 70.3 | 68.0 | 3.28 | 1.70 | 7.08 |
| Utah | 65.7 | 68.0 | 64.2 | 68.6 | 71.2 | 70.6 | 2.97 | 3.16 | 6.40 |
| Vermont | 55.7 | 58.8 | 53.9 | 57.0 | 60.1 | 57.5 | 1.30 | 1.30 | 3.61 |
| Virginia | 63.1 | 70.5 | 57.9 | 64.9 | 72.4 | 62.3 | 1.74 | 1.95 | 4.34 |
| Washington | 51.5 | 52.2 | 51.5 | 54.8 | 54.1 | 56.6 | 3.28 | 1.94 | 5.17 |
| West Virginia | 61.6 | 67.2 | 58.9 | 62.6 | 68.3 | 61.1 | 1.03 | 1.02 | 2.27 |
| Wisconsin | 60.1 | 62.5 | 58.6 | 64.3 | 64.2 | 67.6 | 4.26 | 1.76 | 9.05 |
| Wyoming | 57.2 | 58.3 | 57.1 | 59.9 | 59.9 | 62.1 | 2.70 | 1.59 | 5.01 |

Table S3: Feature inputs of machine learning models. All variables are at daily resolution, except for population, elevation, and land cover (which are time-invariant). All variables are regridded to 10 km for model training and predictions.

| **Type** | **Feature** | **Resolution** | **Source** |
|---|---|---|---|
| Meteorology | Temperature (Min, Max, Mean)<br>Dewpoint (Min, Max, Mean)<br>Surface pressure<br>Wind (U, V, speed, direction)<br>Precipitation<br>Soil moisture<br>LAI (High and Low vegetation) | 9 km | ERA5-Land (*75*) |
| | Mean sea level pressure<br>UV radiation<br>Total cloud cover<br>Total column ozone<br>Boundary layer height | 25 km | ERA5 (*74*) |
| $O_3$ Precursor | $NO_2$ (at 1000 hPa level)<br>Formaldehyde (at 1000 hPa level) | 75 km | CAMS (EAC4) (*73*) |
| Geography | Land cover (resampled to 10 categories: Water, Forest, Shrub, Savanna, Grass, Wetland, Crop, Urban, Ice, Barren)<br>Distance to water | 5 km | MCD12C1 (MODIS) |
| | Elevation | 1 km | EarthEnv (*76*) |
| | Population | 1 km | Gridded EIF (*78*) |
| Fire | Fire radiative power (FRP)<br>Distance to fire | points | FIRMS (MODIS C6.1) |
| | Smoke $PM_{2.5}$ | 10 km | Childs et al. (*19*) |
| Others | Day of the year | – | – |

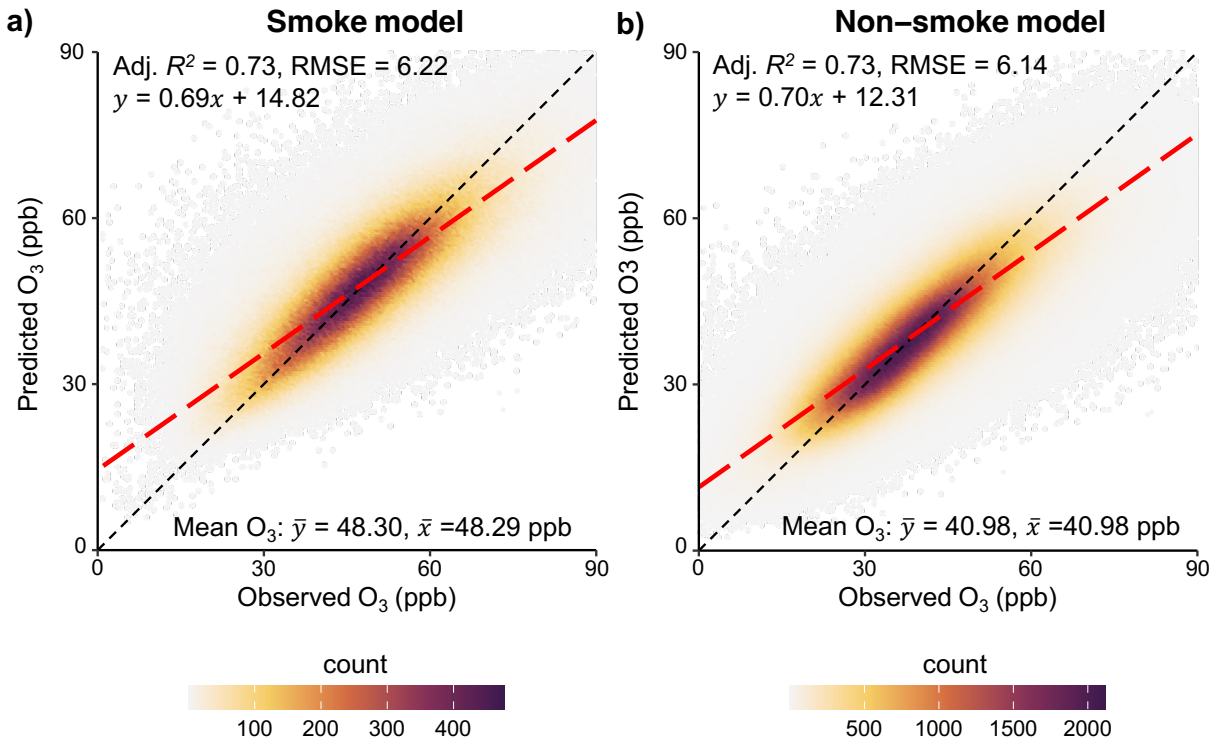


Figure S1: **Out-of-sample performance of ML models.** The figure shows the out-of-sample performance of our smoke and non-smoke ML models in predicting $O_3$ on smoke days and non-smoke days. x-axis shows the observed daily MDA8 $O_3$ concentration, and y-axis shows the predicted concentrations. The mean of observed and predicted $O_3$ concentrations, best linear fits (red line), $R^2$, and root mean squared error (RMSE) are shown in the figure. 1:1 line is shown in dashed black.

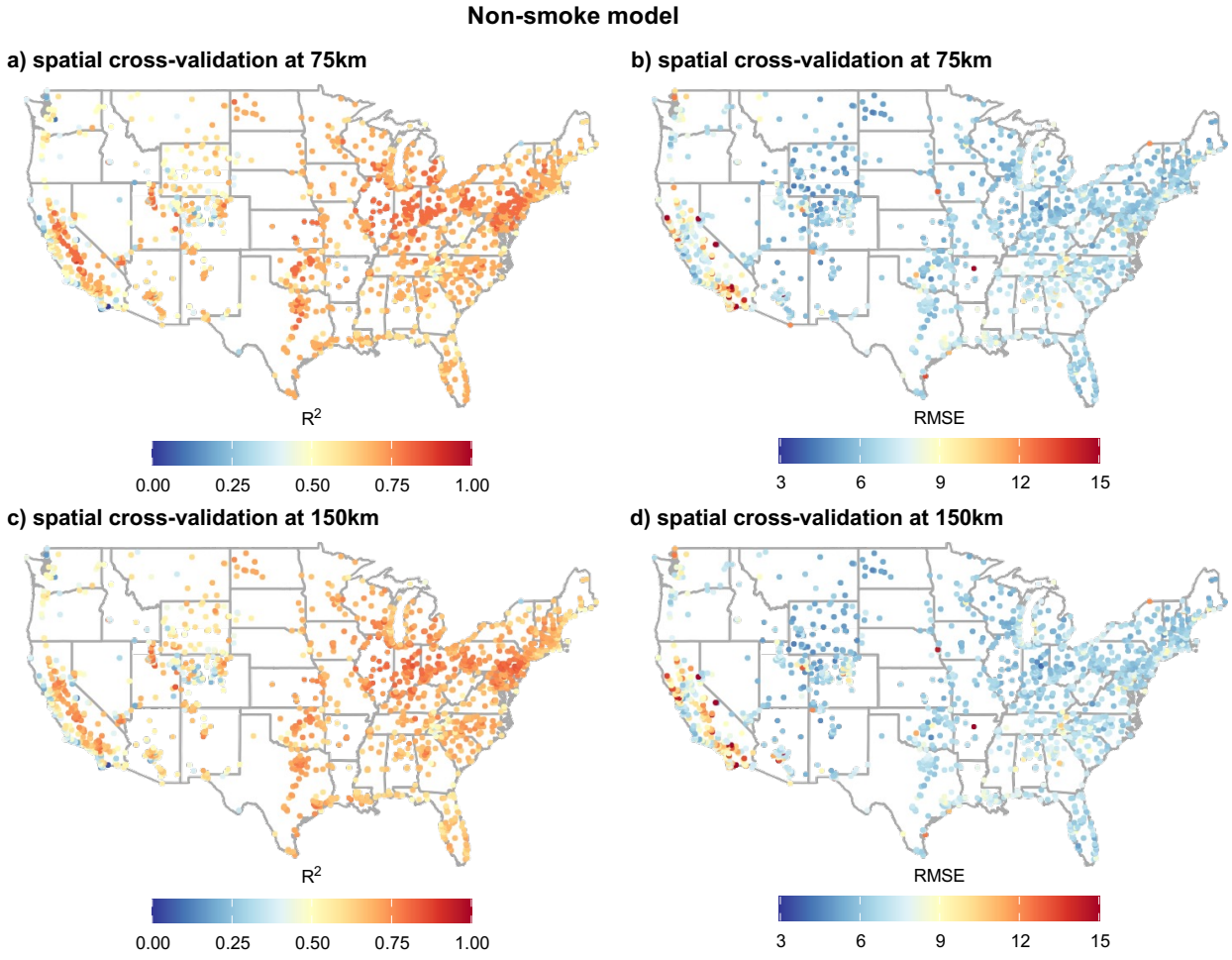


Figure S2: **Model performance of non-smoke ML models.** The figure shows the out-of-sample performance of our non-smoke ML models in predicting $O_3$ on non-smoke days at each monitoring station. $R^2$ and root mean squared error (RMSE) are shown in the figure. Results are shown for two spatial cross-validation splits, with the split defined as 75km (a, b) or 150km (c, d).

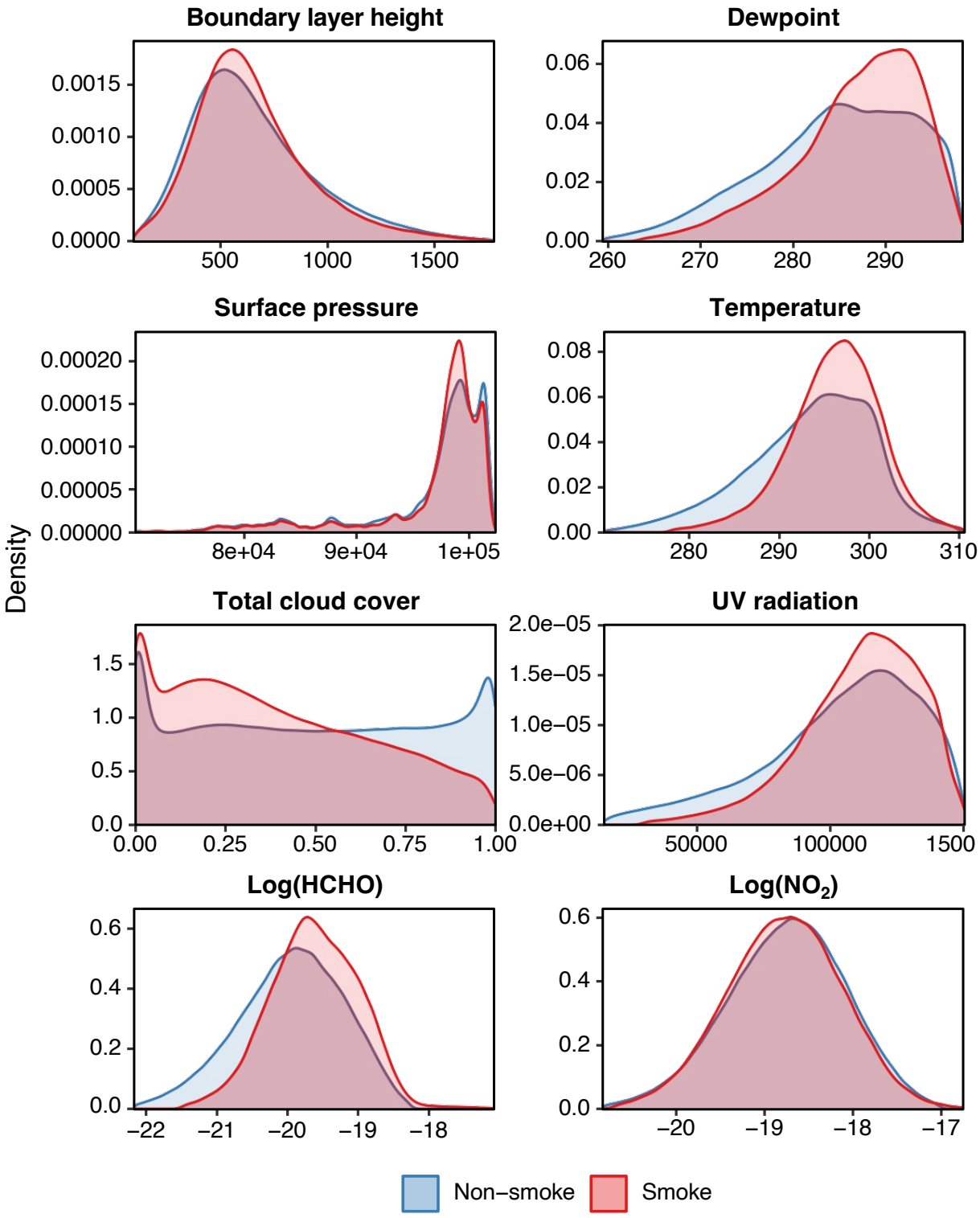


Figure S3: **Distribution of predictors across smoke and non-smoke days.** Density distributions of the eight input predictors used in the ML models, compared between smoke and non-smoke days. Non-smoke days are limited to those in the warm season to be more comparable to smoke days.

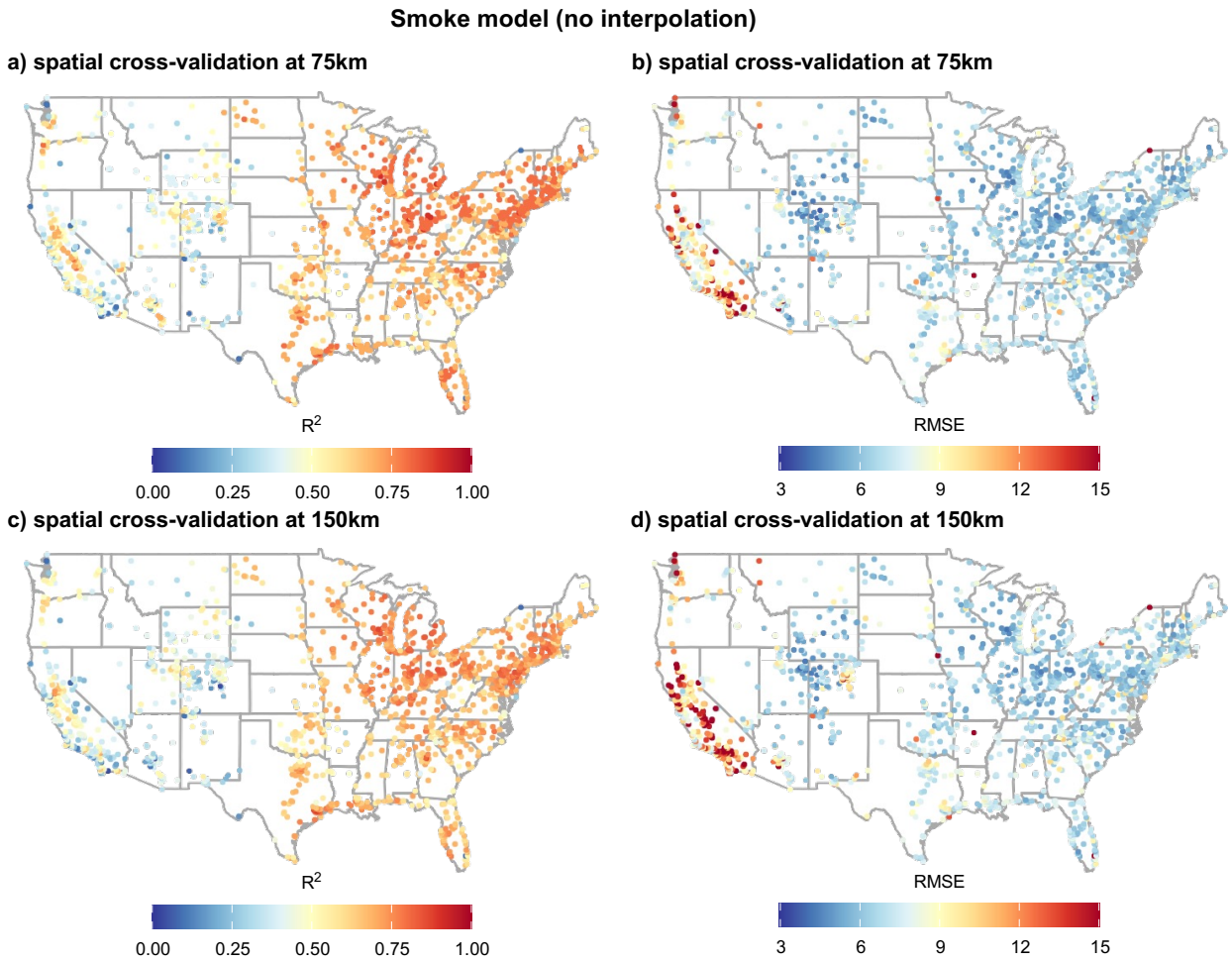


Figure S4: **Model performance of smoke ML models (without using interpolation).** The figure shows the out-of-sample performance of our smoke ML models in predicting $O_3$ on smoke days at each monitoring station. Importantly, the model does not include interpolated $O_3$ concentrations from the station data. $R^2$ and root mean squared error (RMSE) are shown in the figure. Results are shown for two spatial cross-validation splits, with the split defined as 75km (a, b) or 150km (c, d).

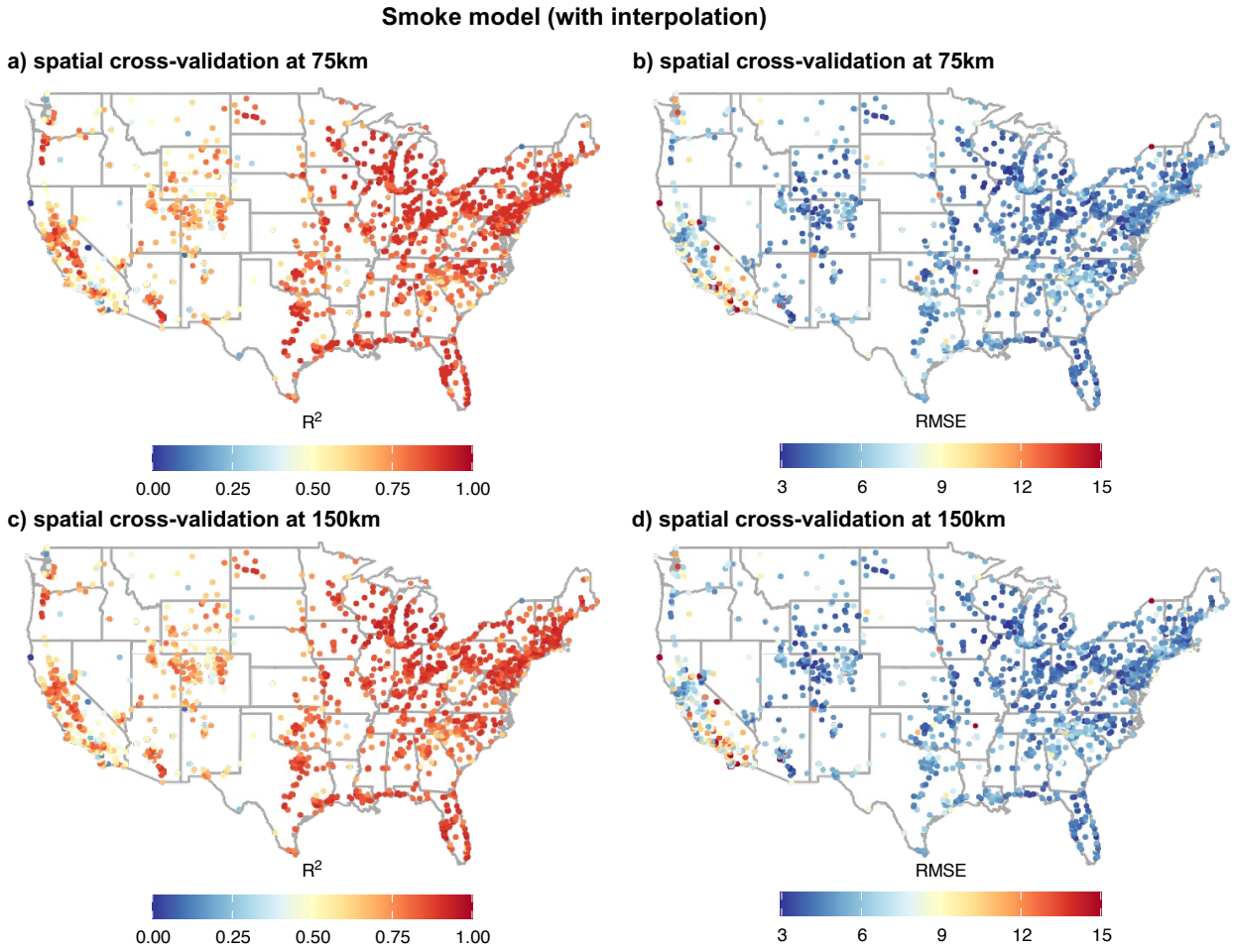


Figure S5: **Model performance of smoke ML models (using interpolation).** The figure shows the out-of-sample performance of our smoke ML models in predicting $O_3$ on smoke days at each monitoring station. Importantly, the model includes interpolated $O_3$ concentrations from the station data as a feature. $R^2$ and root mean squared error (RMSE) are shown in the figure. Results are shown for two spatial cross-validation splits, with the split defined as 75km (a, b) or 150km (c, d).

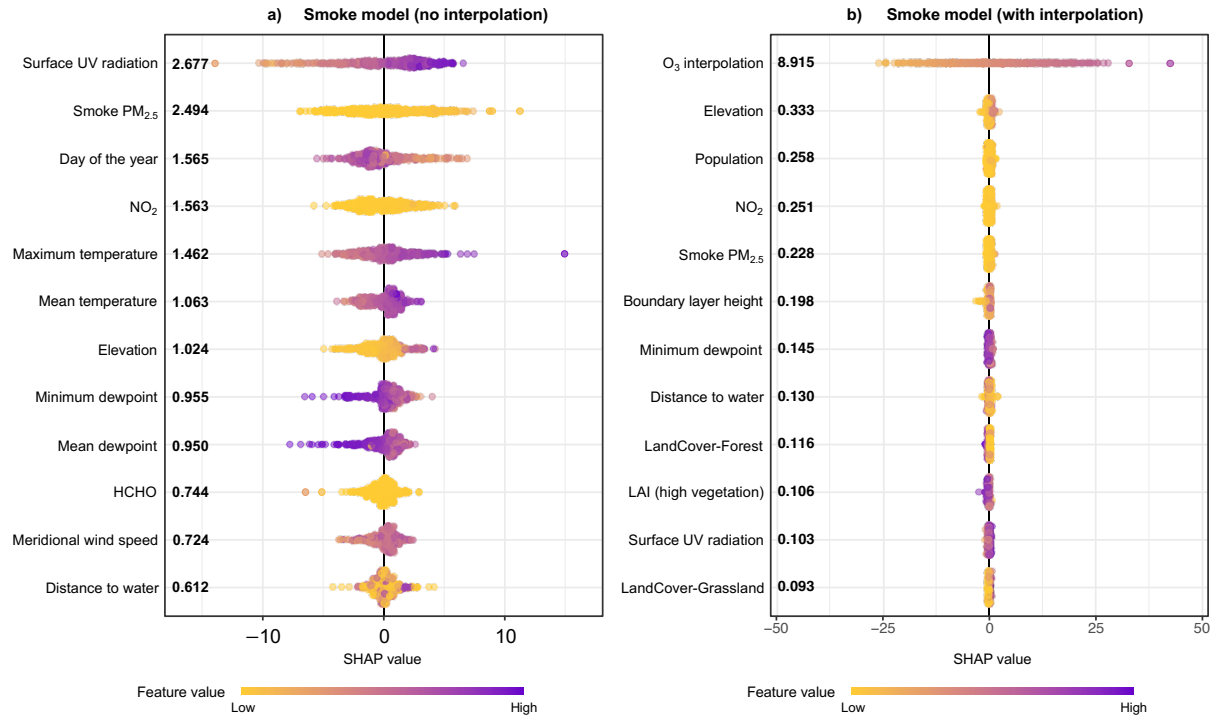


Figure S6: **SHAP value based variable importance for XGBoost smoke models.** Panel a: smoke model (no interpolation). Panel b: smoke model (with interpolation). The SHAP value represents the impact of each feature on the model's prediction relative to the baseline. A larger SHAP value indicates a greater contribution of the feature to model's output, either positively or negatively. Each listed number corresponds to the feature importance, defined as the absolute mean of all SHAP values for a specific feature, reflecting the model's sensitivity to each individual feature. The distribution of points along the horizontal axis shows the range of SHAP values for each feature, with individual points representing the contribution to each observation. The color of the points represents the value of the feature, with low feature values in yellow and high feature values in purple.

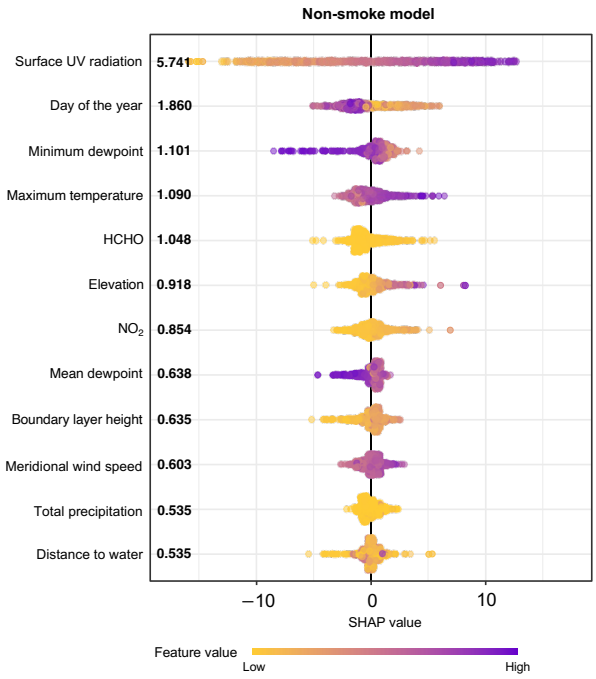


Figure S7: **SHAP value based variable importance for XGBoost non-smoke model.** The SHAP value represents the impact of each feature on the model's prediction relative to the baseline. A larger SHAP value indicates a greater contribution of the feature to model's output, either positively or negatively. Each listed number corresponds to the feature importance, defined as the absolute mean of all SHAP values for a specific feature, reflecting the model's sensitivity to each individual feature. The distribution of points along the horizontal axis shows the range of SHAP values for each feature, with individual points representing the contribution to each observation. The color of the points represents the value of the feature, with low feature values in yellow and high feature values in purple.

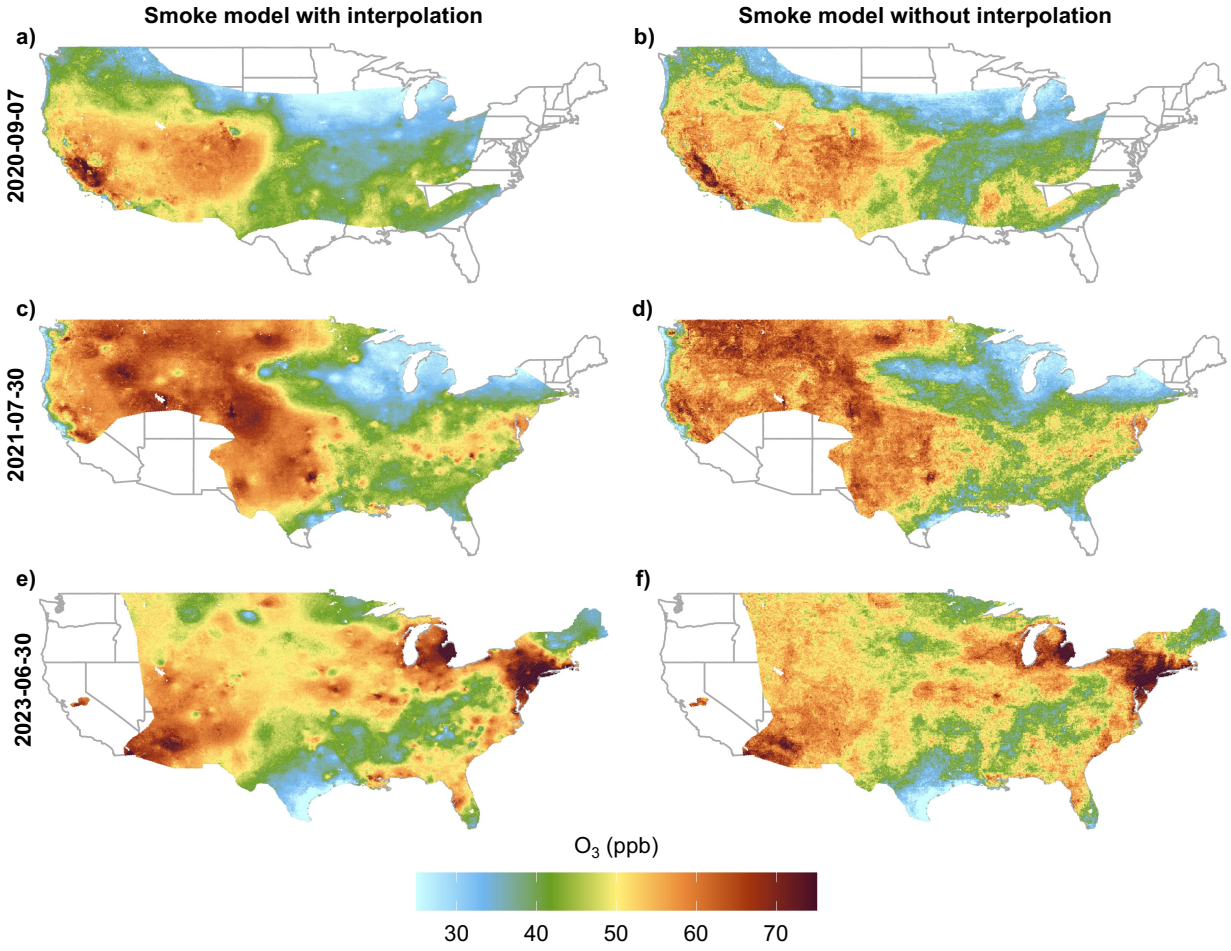


Figure S8: **Spatial patterns of smoke $O_3$ predictions across interpolation and non-interpolation models (selected smoke days).** The plot shows predictions of $O_3$ concentrations on three selected smoke days, from the smoke model with interpolation incorporated, and the smoke model without interpolation.

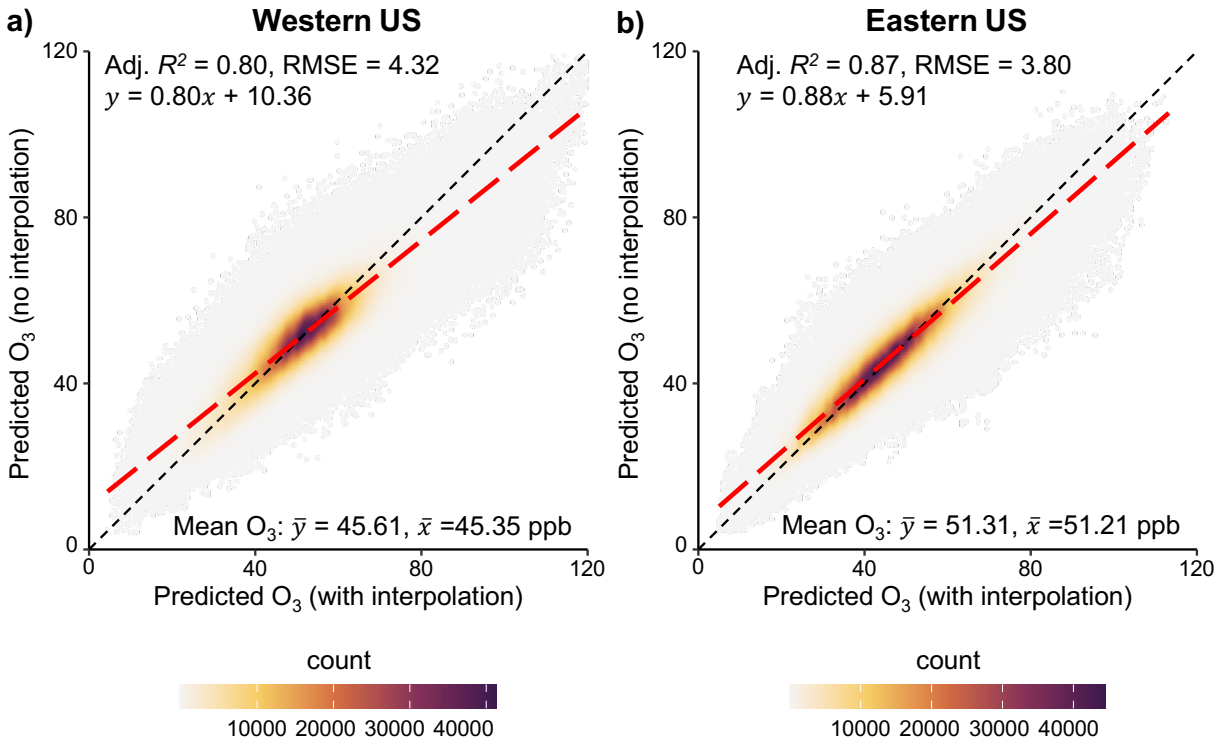


Figure S9: **Comparing smoke $O_3$ estimated across models with and without interpolation.** The plot shows predictions of $O_3$ concentrations on smoke days in western and eastern U.S., across models with and without using the interpolations. The y-axis shows the $O_3$ predictions from ML models without using interpolations (i.e. our main model), and the x-axis shows the $O_3$ predictions from ML models using interpolations. The western U.S. is defined as locations west of the meridian 100° west.

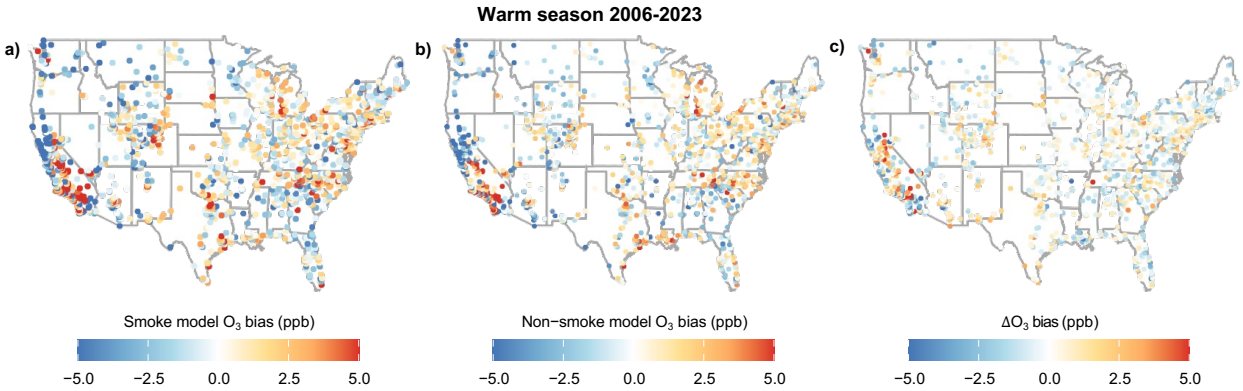


Figure S10: **Prediction bias of $O_3$ concentrations across monitor locations over the warm season.** The plot shows prediction bias (defined as *predictions* - *observed*) averaged over the warm season (April to September) from 2006-2023, for smoke days (panel a), non-smoke days (panel b), and their differences (panel c).

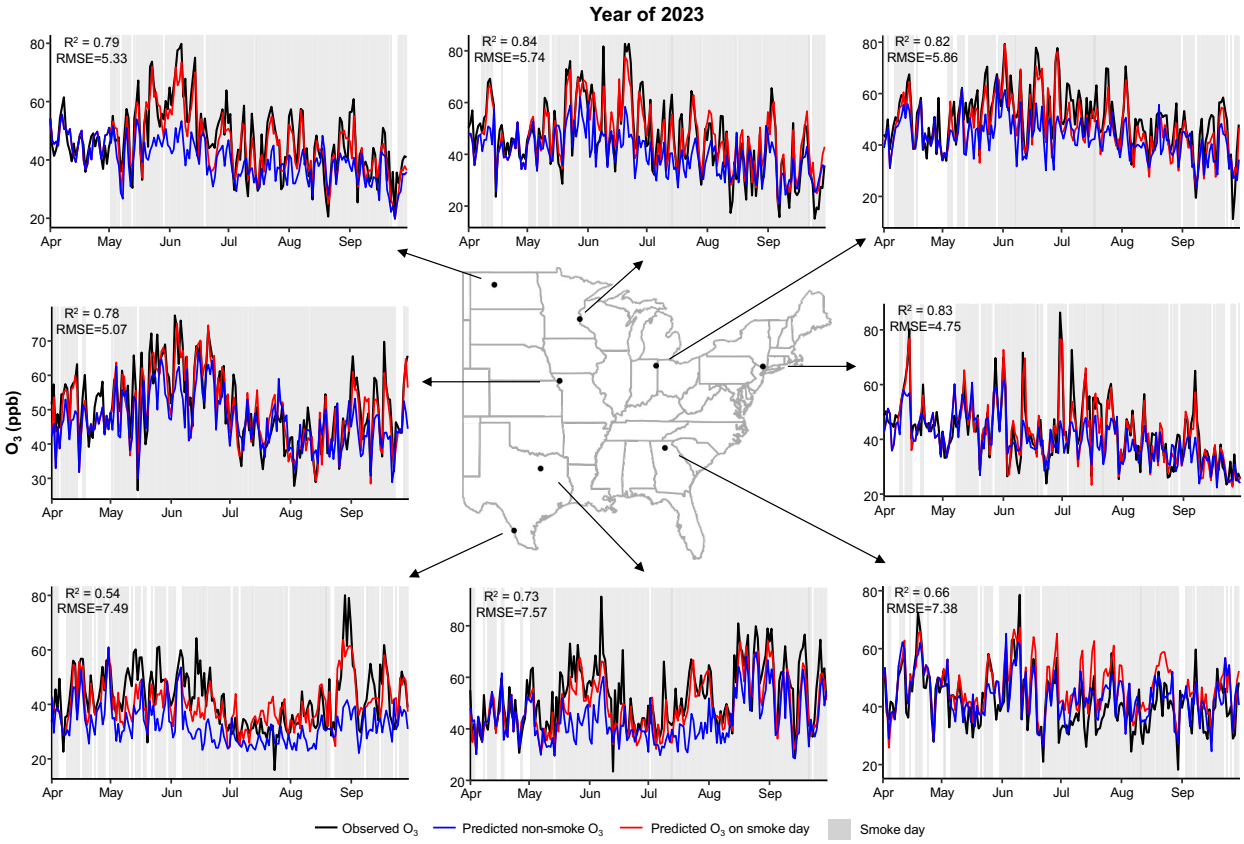


Figure S11: **Observed and predicted daily $O_3$ concentrations at selected monitoring sites.** Black lines show observed total $O_3$ concentrations. Blue lines show estimated counterfactual non-smoke $O_3$ concentrations. Red lines show predicted $O_3$ concentrations on smoke days from the smoke model. Both blue and red lines are out-of-sample predictions from models trained on datasets that excluded the corresponding site. The plot shows $R^2$ and RMSE between observed (black) and predicted $O_3$ concentrations (red line on smoke days + blue line on non-smoke days). Grey shading indicates smoke days identified using HMS smoke polygons.

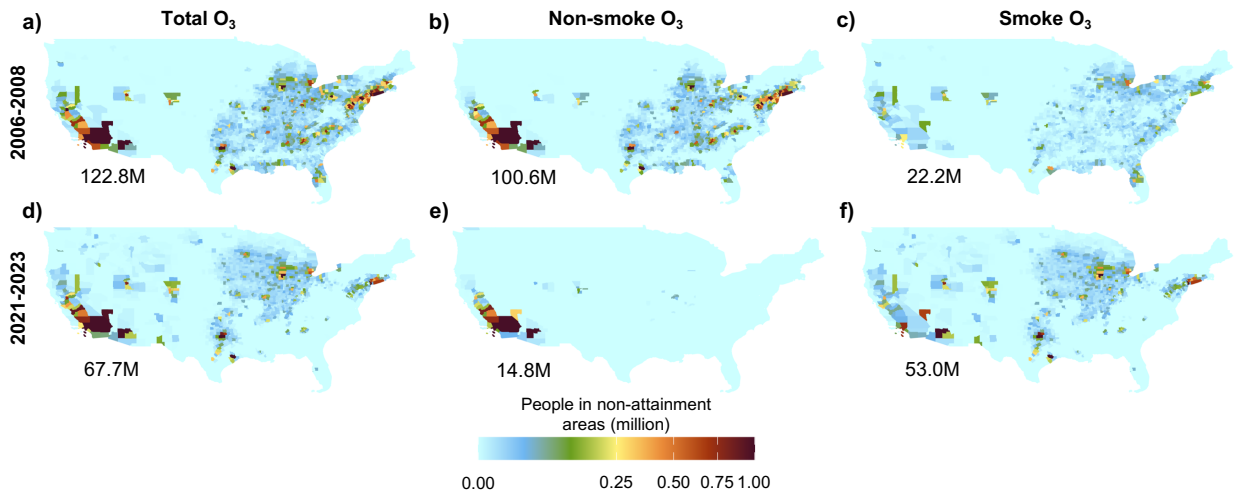


Figure S12: **County-level population in $O_3$ nonattainment areas.** Nonattainment is determined at the grid-cell level if the annual 4th maximum MDA8 $O_3$ concentration exceeds 70 ppb. Panels a, b, and c (top row) show results averaged over 2006-2008. Panels d, e, and f (bottom row) show results averaged over 2021-2023. Panels a and d (first column) show nonattainment based on total $O_3$ concentration (smoke plus non-smoke); panels b and e show nonattainment based on non-smoke $O_3$; panels c and f show the additional population placed in nonattainment by wildfire smoke (the difference between total and non-smoke $O_3$). Total population living in nonattainment areas is shown in the bottom-left corner of each panel.

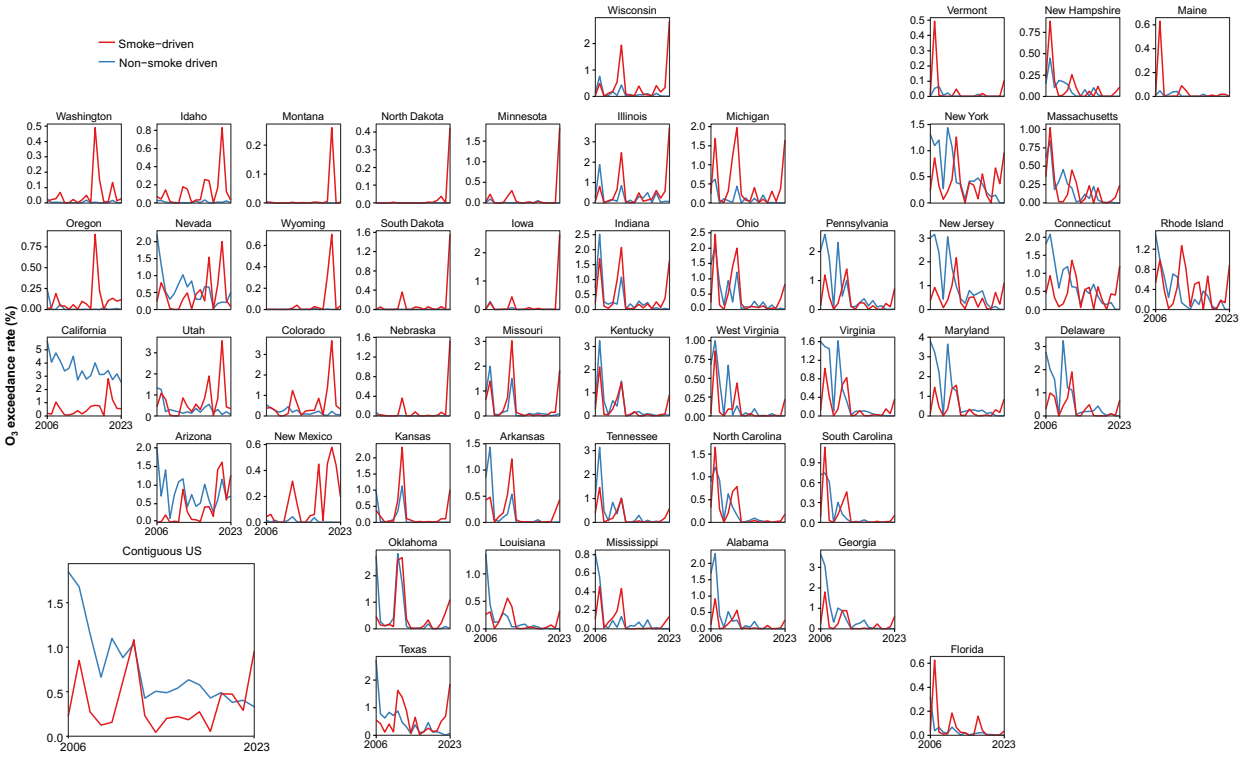


Figure S13: **The influence of wildfire smoke on daily $O_3$ exceedance.** The plot shows the population-weighted fraction of days with MDA8 $O_3 > 70$ ppb for each state. "Smoke-driven" $O_3$ exceedance (red) is defined as days when the baseline non-smoke $O_3$ is below 70 ppb but the total $O_3$ (smoke $O_3$ + baseline) exceeds 70 ppb. "Not smoke-driven" $O_3$ exceedance (blue) is defined as locations and days when the daily non-smoke $O_3$ already exceeds 70 ppb; thus, the exceedance is not due to fire smoke influences.

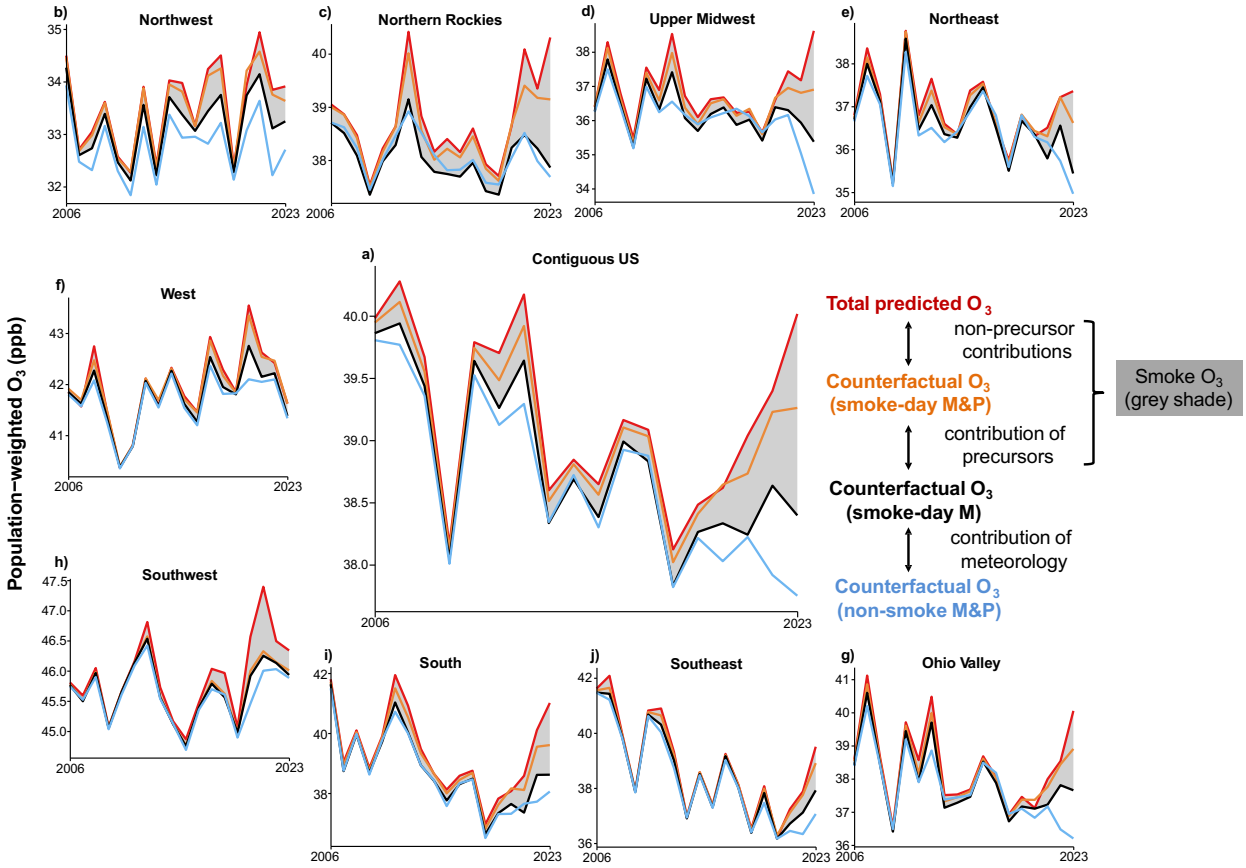


Figure S14: **The influence of fire smoke on population-weighted annual average $O_3$ across U.S. regions.** Red lines show annual population-weighted averages for predicted total $O_3$ (both smoke and non-smoke). Orange lines show estimated counterfactual $O_3$ on smoke days using smoke day meteorology (M) and precursor (P) conditions. Differences between red and orange lines represent the contributions of smoke to $O_3$ from non-precursor changes. Black lines show estimated counterfactual $O_3$ on smoke days using smoke day meteorology (M) but average precursor (P) conditions on non-smoke days. Differences between orange and black lines represent the contributions of smoke to $O_3$ from precursor changes. Blue lines show estimated counterfactual $O_3$ on smoke days using average meteorology (M) and precursor (P) conditions on non-smoke days. Differences between black and blue lines represent the contributions of meteorological variability to smoke day $O_3$ concentrations (note this part is not included to quantify smoke $O_3$ contributions). Gray shading shows the contribution of wildfire smoke to the annual average $O_3$ calculated by subtracting estimated counterfactual non-smoke $O_3$ from total $O_3$ concentrations. The region definition is the same as those in Figure 4.

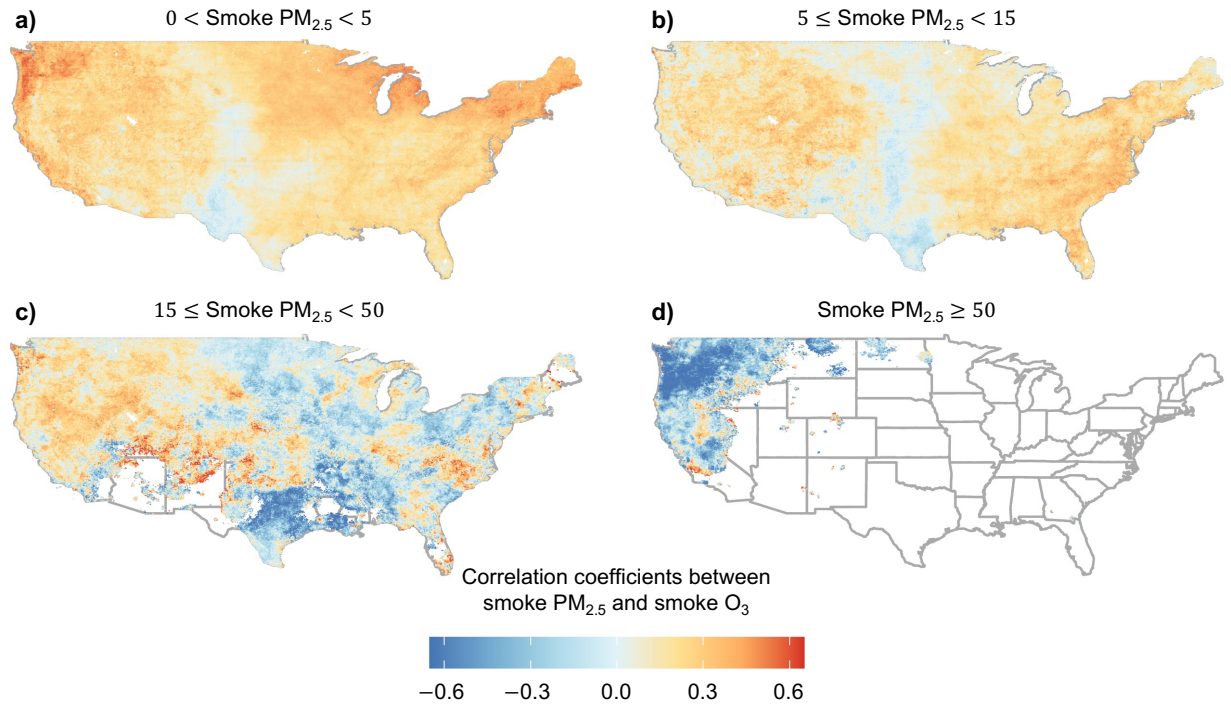


Figure S15: **Varying correlations between daily smoke $PM_{2.5}$ and smoke $O_3$ across different smoke $PM_{2.5}$ levels.** Panels **a**–**d** illustrate the Pearson correlation coefficients between daily smoke $PM_{2.5}$ and smoke $O_3$ within four smoke $PM_{2.5}$ concentration ranges: (**a**) 0–5 $\mu g/m^3$, (**b**) 5–15 $\mu g/m^3$, (**c**) 15–50 $\mu g/m^3$, and (**d**) $\geq$ 50 $\mu g/m^3$.

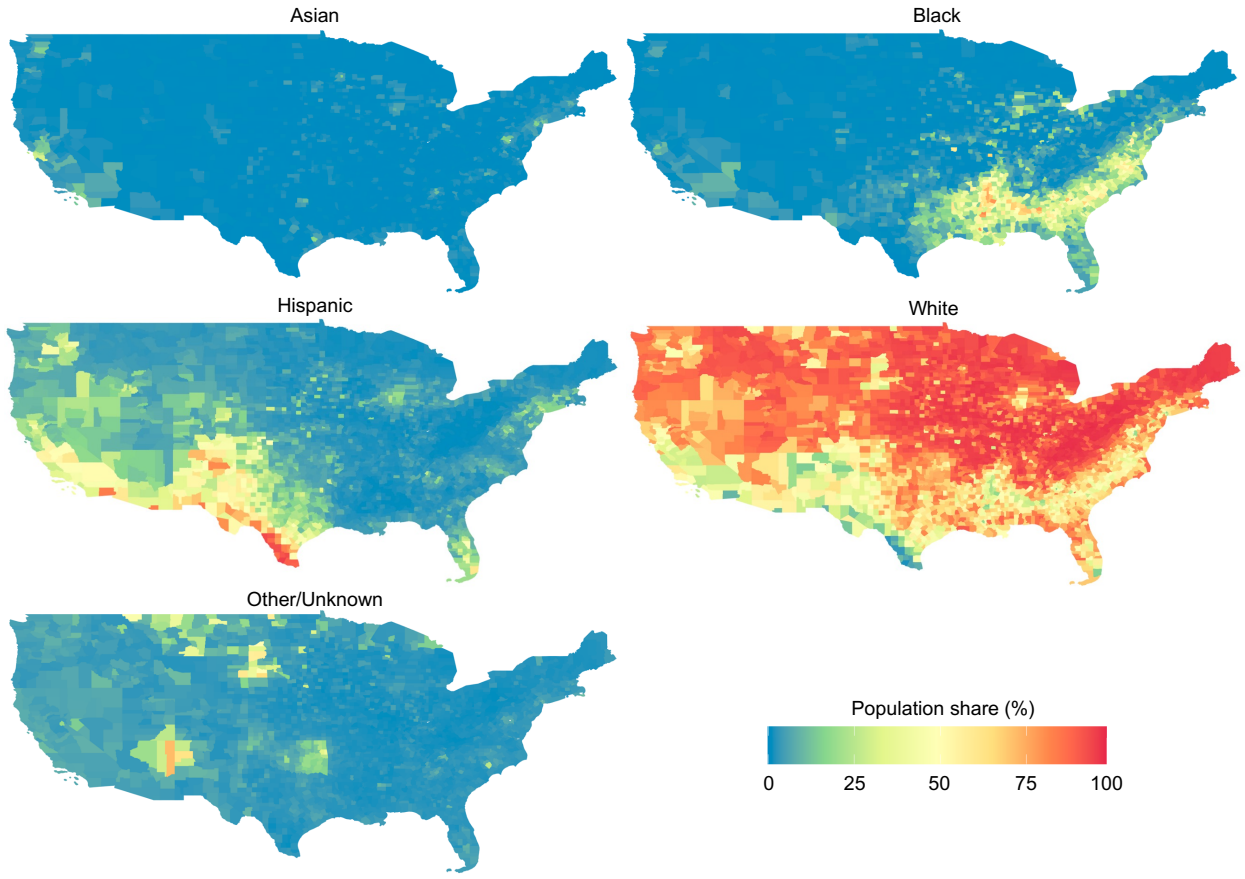


Figure S16: **Geographic distribution of population by race and ethnicity.** The plot illustrates the share of population for the five racial and ethnic groups across the contiguous United States, including Asian, Black, Hispanic, White, and Other/Unknown. The color scale represents the population share (%) within each county belonging to the respective group.

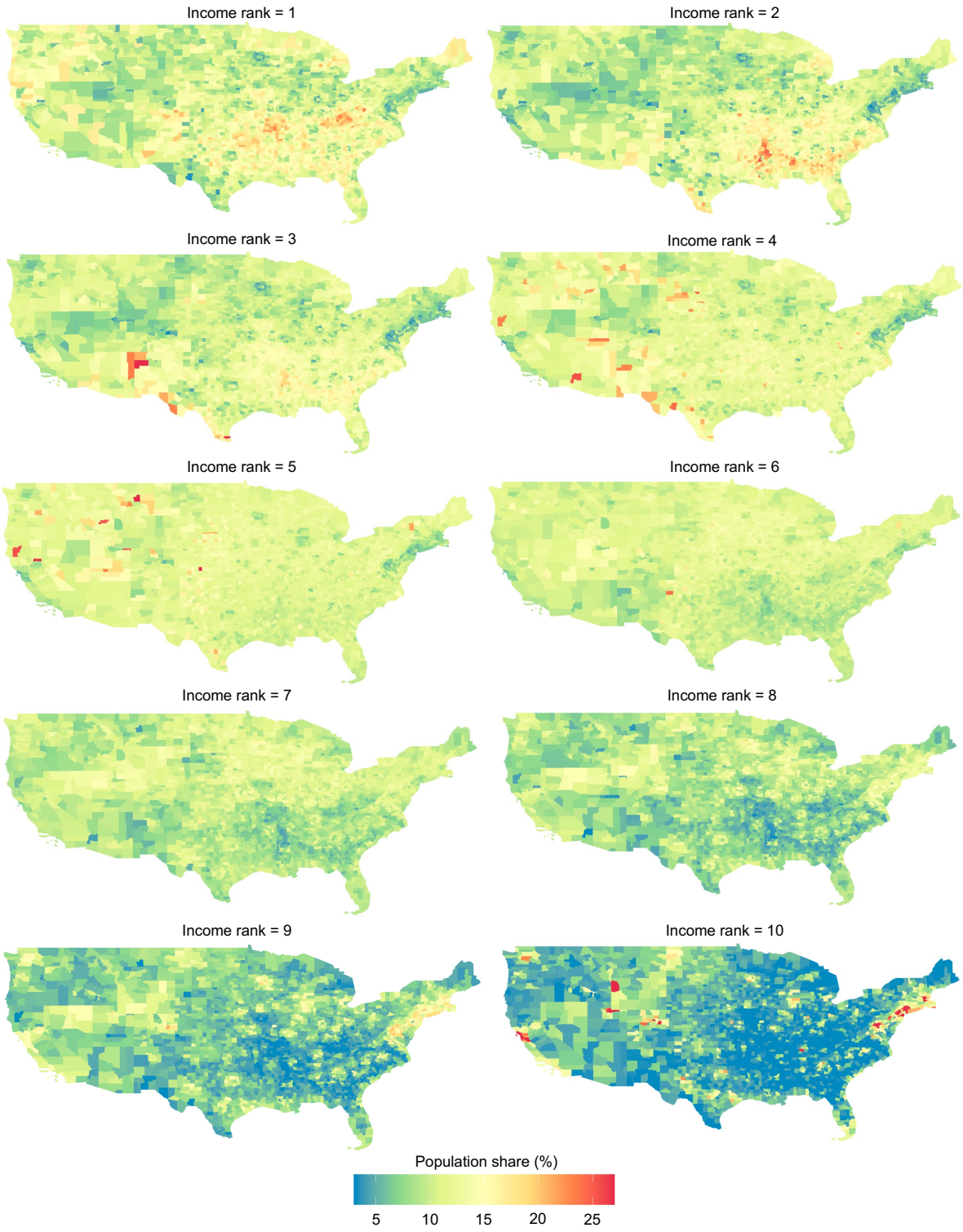


Figure S17: **Geographic distribution of population by income deciles.** Each panel illustrates the share of population for income deciles, ranging from income rank = 1 (lowest income) to income rank = 10 (highest income). The color intensity represents the population share (%) within each county belonging to the respective income decile.

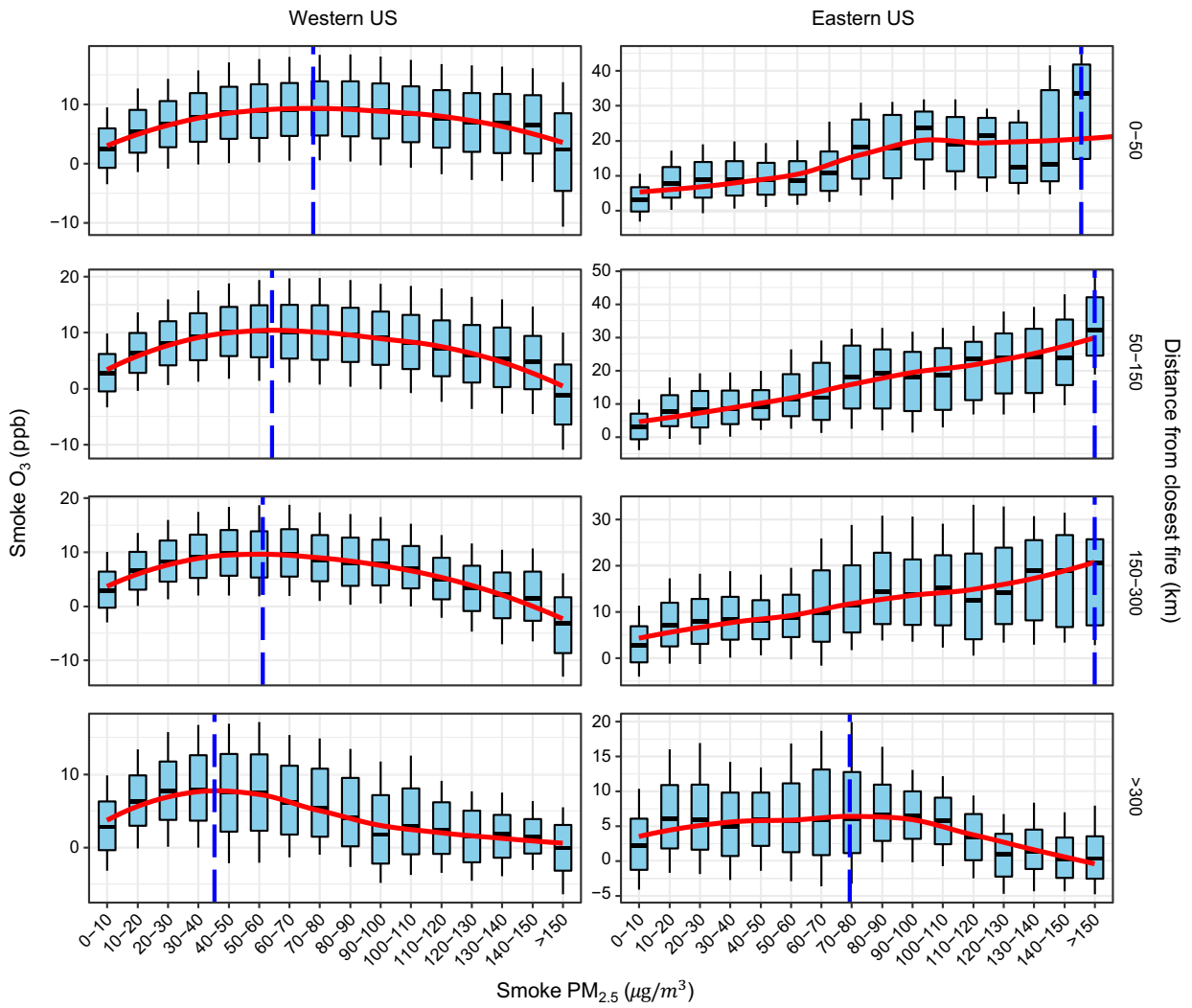


Figure S18: **Non-linear relationship between smoke $PM_{2.5}$ and smoke $O_3$ across different distances to the closest fire.** The boxplots illustrate the distribution of daily smoke $O_3$ at different daily smoke $PM_{2.5}$ bins across different distances to the closest fire: thick black lines represent the medians, box edges denote the 25th and 75th percentiles, and whiskers extend to the 10th and 90th percentiles. The solid red lines represent a LOESS regression fitted to the medians of each box. The vertical dashed blue lines indicate the smoke $PM_{2.5}$ threshold at which smoke $O_3$ concentrations reach their maximum value (i.e. the turning points). Fire distances are calculated as the distance from the grid cell to the closest fire point on the same day.

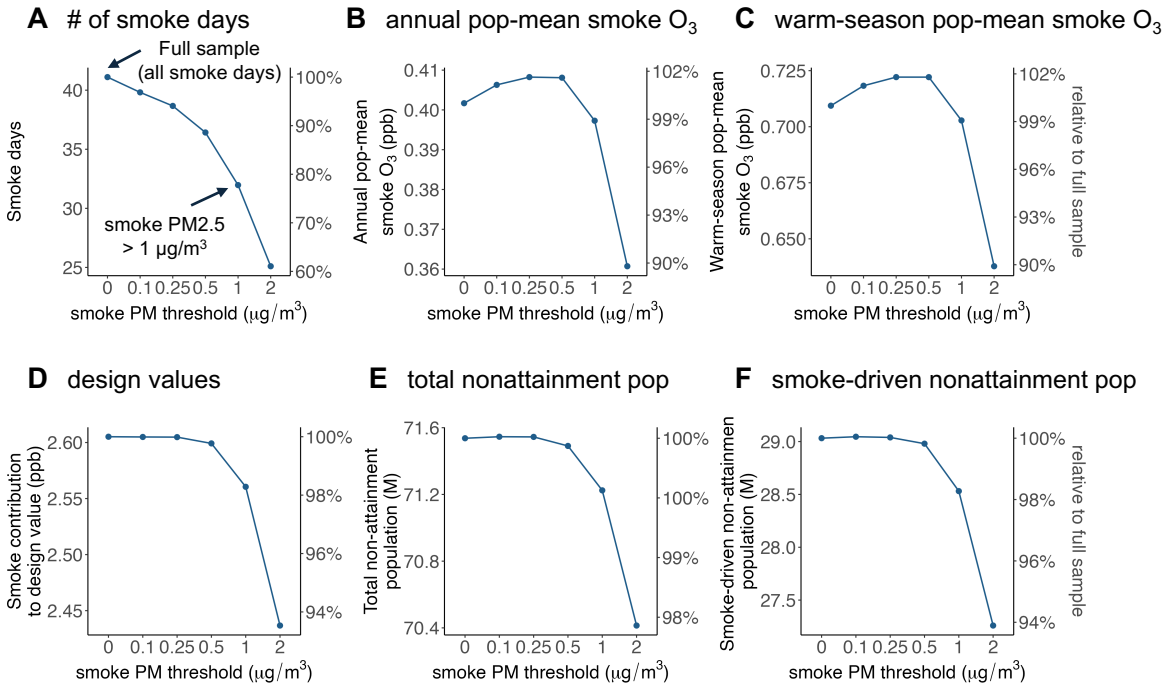


Figure S19: **Results across alternative smoke-day identification thresholds that exclude low smoke $PM_{2.5}$ days from the smoke-day sample**. The plot shows how outcome variables change as the sample is restricted to smoke days with estimated daily smoke $PM_{2.5} > x$ $\mu g/m^3$ (x-axis). Outcomes examined include the number of identified smoke days (panel A), estimated annual and warm-season population-weighted smoke $O_3$ (B and C), the smoke contribution to annual mean design values (D), the total population in $O_3$ nonattainment areas (E), and the additional population in nonattainment areas due to wildfire smoke (F). Smoke $PM_{2.5}$ estimates are derived from Childs et al. 2024 (*19*).